Nat. Hazards Earth Syst. Sci., 24, 3129–3154, 2024
https://doi.org/10.5194/nhess-24-3129-2024

Natural Hazards and Earth System Sciences
Open Access
EGU

Forearc crustal faults as tsunami sources in the upper plate of the Lesser Antilles subduction zone: the case study of the Morne Piton fault system

Melody Philippon[1], Jean Roger[2], Jean-Frédéric Lebrun[1], Isabelle Thinon[3], Océane Foix[4], Stéphane Mazzotti[4], Marc-André Gutscher[5], Leny Montheil[4], and Jean-Jacques Cornée[4]

[1]Géosciences Montpellier, Université de Montpellier, CNRS, Université des Antilles, Pointe-à-Pitre, French West Indies, France
[2]Earth and Structure Processes Department, GNS Science, Lower Hutt, New Zealand
[3]BRGM – French geological survey, 3 avenue Claude Guillemin, 45060 Orléans, France
[4]Géosciences Montpellier, Université de Montpellier, CNRS, Université des Antilles, Montpellier, France
[5]Geo-Ocean, Univ. Brest, CNRS, Ifremer, Brest, France

Correspondence: Melody Philippon (melody.philippon@univ-antilles.fr)

Received: 16 December 2023 – Discussion started: 22 January 2024
Revised: 7 May 2024 – Accepted: 21 June 2024 – Published: 19 September 2024

Abstract. In this study, alternatively to the megathrust, we identify upper-plate normal faults orthogonal to the trench as a possible tsunami source along the Lesser Antilles subduction zone. The Morne Piton fault system is such a trench-perpendicular upper crustal fault at the latitude of Guadeloupe. By means of seismic reflection, high-resolution bathymetry, remotely operated vehicle (ROV) imaging and dating, we reassess the slip rate of the Morne Piton fault since 7 Ma, i.e., its inception, and quantify an average rate of 0.25 mm yr^{-1} since ca. 1.2 Ma. This result divides by two previous estimations, increases the earthquake time recurrence and lowers the associated hazard. The ROV dive revealed a metric scarp with striae at the toe of the Morne Piton fault system, suggesting a recent fault rupture. We estimate a fault rupture area of $\sim$450–675 km^2 and then a magnitude range for a maximum seismic event around M_w 6.5 ± 0.5, making this fault potentially tsunamigenic as the nearby Les Saintes fault responsible for a tsunami following the 2004 M_w 6.3 earthquake. Consequently, we simulate a multi-segment tsunami model representative of a worst-case scenario if all the identified Morne Piton fault segments ruptured together. Our model provides clues for the potential impact of local tsunamis on the surrounding coastal area as well as for local bathymetric controls on tsunami propagation. We illustrate that (i) shallow-water plateaus act as secondary sources and are responsible for a wrapping of the tsunami waves around the island of Marie-Galante; (ii) canyons indenting the shallow-water plateau slope break focus and enhance the wave height in front of the most touristic and populated town of the island; and (iii) the resonance phenomenon is observed within the Les Saintes archipelago, showing that the waves' frequency content is able to perturb the sea level for many hours after the seismic rupture.

1 Introduction

Regions in the vicinity of active subduction zones are prone to seismic and related hazards, including tsunamis, exposing their inhabitants to multiple threats. Megathrust earthquakes represent the greatest threat with the highest seismic moments and consequently huge tsunamigenic potential (Satake and Tanioka, 1999). Earthquakes triggered on crustal faults in the overriding plate represent an additional hazard that needs to be quantified (Bilek, 2010). In order to assess the hazards and mitigate the risks associated with these crustal faults, it is essential to estimate their slip rates.

On land, slip rates on active faults are determined from paleo-seismic trenches (McCalpin, 1996), high-resolution geophysical investigation (Wallace, 1981; Zhang et al.,

2014), satellite imagery (Tronin, 2009), InSAR (Biggs and Wright, 2020), geodetic measurement (GNSS, Symithe et al., 2013) and seismicity, which account for the present-day strain accumulation of the crust. Offshore, slip rate estimates are provided by means of underwater geodesy (i.e., acoustic geodesy, Kido et al., 2006; Petersen et al., 2019; Fujita et al., 2006) or fiber optic monitoring (Hirata et al., 2002; Gutscher et al., 2019). The recurrence time of events may be estimated by the study of turbidite deposits cores (e.g., Cascades, Goldfinger et al., 2012; Taiwan, Lehu et al., 2016; Antilles, Seibert et al., 2020; New Zealand, Lewis, 1980), high-resolution marine seismic and multibeam echo-sounder data (e.g., Escartín et al., 2016, 2018), and submarine survey dives (e.g., Geli et al., 2011). However, constraining hazard models in areas undergoing slow strain rates remains challenging as the earthquakes' recurrence time overcomes the historical period. Indeed, geodetic measurements require decade-long time series as the resolution of the method is not accurate enough, and erosion or high sedimentation rates may have erased or covered, respectively, the active fault scarps, making it difficult to identify active fault segments. Therefore, datasets based on the last 10 to 100 years of record along tectonic systems undergoing slow strain rates may not be representative of the bulk strain and may be at the origin of biased estimations of the slip rate along these faults.

The Lesser Antilles (eastern Caribbean) records show slow deformation rates as the North and South American tectonic plates slowly subduct under the Caribbean plate ($20\,\mathrm{mm\,yr^{-1}}$, Fig. 1). Extensional tectonics and normal faulting affect the forearc (Feuillet et al., 2002; De Min et al., 2015; Boucard et al., 2021), but available historical data do not report tsunami events related to forearc fault rupture. However, the Les Saintes M_w 6.3 earthquake of December 2004 ruptured the Roseau normal fault (Feuillet et al., 2011; Bazin et al., 2010). The earthquake reached an intensity up to VIII in the Guadeloupe archipelago (Fig. 1), was felt by most of its $\sim 400\,000$ inhabitants and was responsible for one casualty. This earthquake triggered a tsunami with up to 2 m high waves at the coast and a maximum measured run-up distance of 42 m in Les Saintes (Zahibo et al., 2005; Le Friant et al., 2008; Cordrie et al., 2020). Prior to this event, this fault was unmapped and therefore not identified as an active fault (Feuillet et al., 2002; Terrier et al., 2002). Forearc normal faults, similar to Les Saintes fault system, may pose a threat to the 4 million inhabitants of the Lesser Antilles that are living on volcanic arc islands facing the subduction trench to the east and literally sitting over the subduction interface.

The present study focuses on the Morne Piton fault system, perpendicular to the subduction trench, which is one of the most prominent onshore–offshore fault systems and cuts the Guadeloupe archipelago arc and forearc islands (Fig. 1). Regarding the seismic and tsunami hazards related to this fault system and the vulnerability of the coastal population and infrastructures of the archipelago, the objectives are to (1) estimate the fault slip rate; (2) determine the geometry of the fault segments; and (3) model the associated tsunami hazard, since such a joint approach has been lacking so far.

In this paper, the fault geometry is refined in order to provide an up-to-date map of the fault segments thanks to high-resolution (HR) bathymetric data. Then, we integrate its long-term slip rate over the last ca. 7 Myr, i.e., from fault initiation to the present day, by means of HR seismic reflection lines and available biostratigraphic and isotopic dates. Secondly, remotely operated vehicle (ROV) explorations of seafloor rupture allowed us to measure the height of the fault scarp and to determine the fault kinematics from striations observed along a recent coseismic scarp. Because the overall geometry of this fault system is comparable to the Les Saintes fault system in terms of length, seafloor scarp and dip, we postulate that a rupture along the Morne Piton fault may trigger a local tsunami close to the coasts of the Guadeloupe archipelago. Therefore, we study the seismogenic and tsunamigenic potential of the Morne Piton fault system, providing an overview of what could happen in terms of tsunami generation if all the segments of the Morne Piton fault ruptured simultaneously, i.e., a plausible worst-case scenario. This scenario allows us to identify and discuss the local bathymetric controls on the propagation of the resulting tsunami wave and the consequences (e.g., amplifications and interferences) in near-shore areas of the neighboring populated islands. We do not assess coastal inundation scenarios, as our scenario cannot be refined by observational rupture data accurate enough to realize such a specific hazard study. Finally, we conclude on the importance of forearc crustal faults as potential major tsunami sources in subduction zones.

2 Geological settings

Oceanic lithosphere of the North and South American plates is slowly subducting beneath the Caribbean plate at a convergence rate of $\sim 20\,\mathrm{mm\,yr^{-1}}$ (Fig. 1, DeMets et al., 2000; Philippon and Corti, 2016). The convex trench geometry results in along-strike variations in obliquity, increasing northward from Guadeloupe. Along the arc, oblique subduction is accommodated by trench-parallel left-lateral strike-slip faults such as the Montserrat–Havers–Bouillante and Les Saintes corridor (located within the volcanic arc), the Bunce fault (located along the crustal buttress) and a series of trench-perpendicular grabens forming a sinistral horsetail (Feuillet et al., 2002, 2010; ten Brink et al., 2004; Boucard et al., 2021; Figs. 1, 2a).

In the central Lesser Antilles, the Marie-Galante basin (Guadeloupe archipelago) is located at the southern end of the aforementioned regional horsetail system and is described as a conjugated normal fault system defining a trench-perpendicular graben (Fig. 2a; Feuillet et al., 2001, 2011). This graben affects sediment deposits comprising three regional mega-sequences: an Eocene–Early Miocene

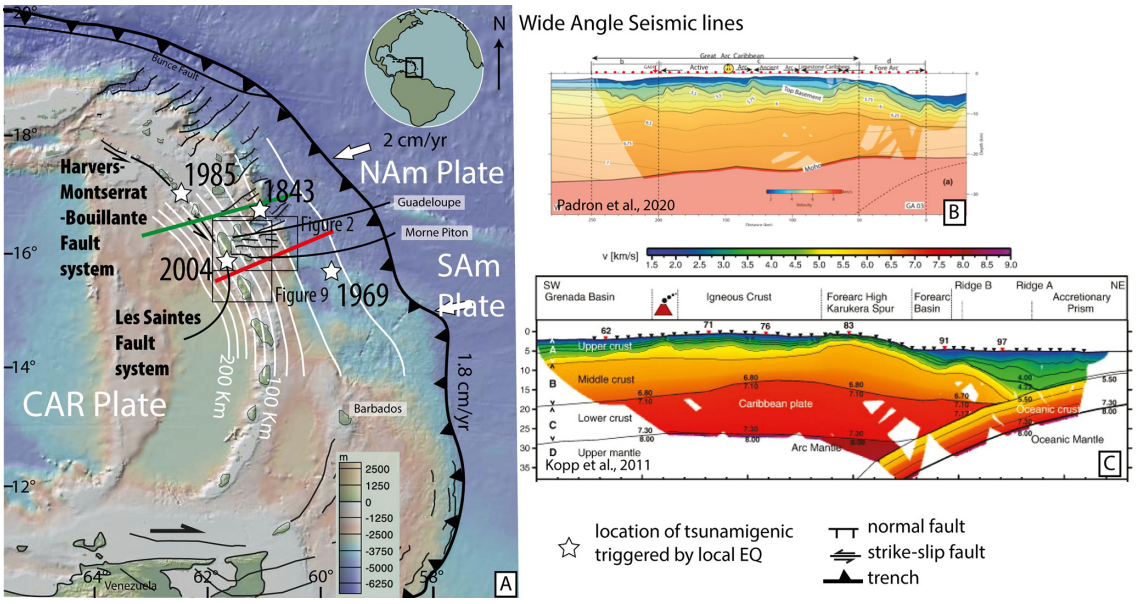

Figure 1. (a) Synthetic tectonic map of the Lesser Antilles forearc. Structures after Feuillet et al. (2002), Legendre et al. (2018) and Boucard et al. (2021). Thick red and green lines indicate the location of the wide-angle seismic lines from **(b)** Kopp et al. (2011) and **(c)** Padron et al. (2021), respectively. White star: location of tsunamigenic earthquakes. Thick white contour lines: slab depth isocontour from Bie et al. (2020).

MG-MS1 sequence, a Middle Miocene–late Tortonian/early Messinian MG-MS2 sequence and a Messinian–present MG-MS3 sequence (Bouysse et Mascle, 1994; De Min et al., 2015; Cornée et al., 2023). It shapes the Marie-Galante basin (up to 1200 m water depth) and surrounding Grande-Terre and Marie-Galante islands (Fig. 1). The northern boundary of the Marie-Galante basin is the east-trending, south-dipping Gosier fault that runs primarily onshore along the southern coast of Grande-Terre (Garrabé and Andreieff, 1988; Fig. 2a). The southern boundary of the basin consists of the N100° E-trending, ∼ 50 km long, north-dipping Morne Piton fault, which crosscuts the northern edge of Marie-Galante island (Bouysse et al., 1993) and extends offshore on both sides of the island (Feuillet et al., 2002, 2004).

The Morne Piton fault system consists of five main 5–15 km long segments trending N90° E ± 30° separated by N140° E shorter right-lateral relays (Fig. 2). The fault scarp is exposed at Anse Piton, eastern coast of Marie-Galante, and shows dip-slip striations (Feuillet et al., 2002). Onshore Marie-Galante, the fault offsets the Pliocene to Middle Pleistocene platform by ∼ 60 m. It also crosscuts a series of three uplifted late Middle to Late Pleistocene terraces along the eastern side of the island. Feuillet et al. (2004) calculated a 5 km dislocation depth and a 70 to 80° N fault dip to model the observed flexure of the footwall. Considering that the Marie-Galante plateau is a flat abandoned 330 ka marine terrace, these authors estimate the average slip rate of the Morne Piton at about 0.5 ± 0.2 mm yr^{-1} since 330 ka. Regarding the uplifted terraces, they estimated a maximum earthquake moment magnitude (M_w) ranging from 5.8 up to 6.5 with a recurrence time of 400–1000 to 1400–3300 years, respectively (250 km^2 of the estimated ruptured area). Moreover, it was later demonstrated that this plateau emerged between 1.77 and 1.07 Ma (magnetostratigraphic chron 1R2r: Cornée et al., 2012; Münch et al., 2014; De Min et al., 2015; Léticée et al., 2019; Cornée et al., 2021). Note that considering an older age for the plateau emergence would drastically lower the slip rate estimate and increase the recurrence time calculated by Feuillet et al. (2001).

3 Historical seismicity

Upper-plate seismicity in the Marie-Galante basin provided by the (i) CDSA seismic database (Antilles Seismological Data Center, Bengoubou-Valerius et al., 2008; Massin et al., 2021), (ii) IEB mixed database USGS and ISC (https://www.isc.ac.uk, last access: September 2024) (Fig. 2b) and (iii) deployment of ocean-bottom seismometers (OBSs; Ruiz et al., 2013; Bie et al., 2020) shows a widely distributed pattern of moderate-magnitude earthquakes ($M_w \leq 5.3$), with the exception of the 2004 seismic cluster in Les Saintes. Wide-angle seismic (WAS) profiles together with earthquakes data indicate a seismogenic crustal thickness limited to the first 15–20 km west of Marie-Galante, suggesting a brittle–ductile transition at this depth (Kopp et al., 2011; Ruiz et al., 2013; Gonzalez et al., 2017; Padron et al., 2021). Among the very few focal mechanisms available in the Marie-Galante basin (Gonzalez et al., 2017), the 25 February 2014 M_w 3.8 earth-

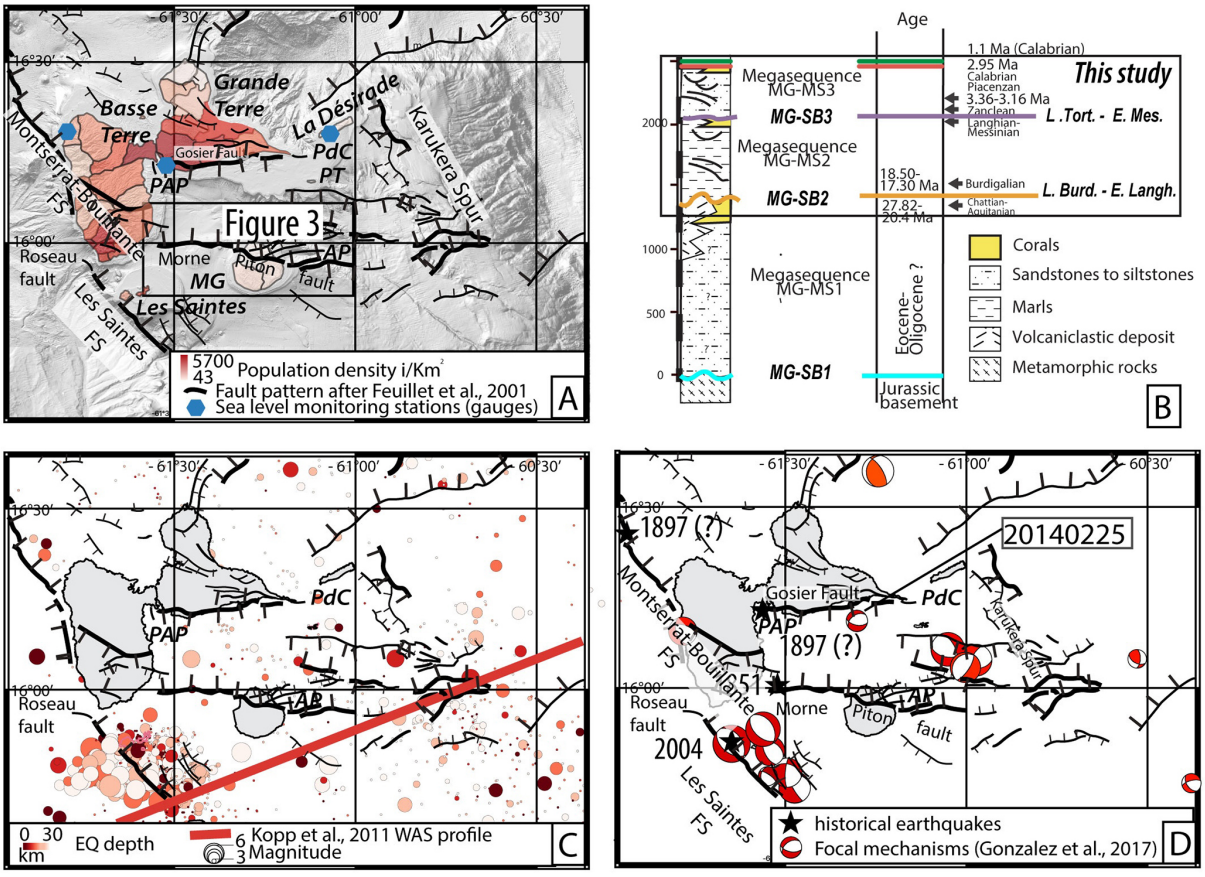

Figure 2. The Marie-Galante basin **(a)** structural pattern after Feuillet et al. (2002) and De Min et al. (2015) on the shaded-relief bathymetric map. Blue hexagons: tide gauges https://data.shom.fr/donnees/refmar/ (last access: October 2022). Red color scale: Guadeloupe population density per square kilometer after GEOFLA (https://www.data.gouv.fr/fr/datasets/geofla-r/, last access: October 2022). **(b)** Seismostratigraphic scheme of the Marie-Galante basin modified after Cornée et al. (2023). **(c)** Colored dots: crustal seismicity from the International Seismological Centre (2023) and USGS (2017) databases for earthquakes (EQ) of magnitude $3 > M_w > 6.5$, located from 0 to 30 km depth; the red line shows the WAS line (Kopp et al., 2011). **(d)** Focal mechanism solutions are indicated by red-and-white beach balls after Gonzalez et al. (2017). The location of historical earthquakes is indicated by black stars (after Feuillet et al., 2011). AP, PdC, PAP and PT stand for Anse Piton, Pointe des Chateaux, Pointe-à-Pitre and Petite-Terre.

quake occurred beneath the southern Grande-Terre platform and shows pure normal motion along sub-E–W-trending nodal planes (Gonzalez et al., 2017; event no. 9; hypocentral location accuracy of ca. 5 km; Fig. 2c). The location, depth and nodal plane characteristics (57° dip and N102° E) of the earthquake indicate that the event may correspond to a rupture along the Gosier fault system, which is the only major fault system in the vicinity of the hypocentral location able to trigger an earthquake of such magnitude. Feuillet (2000) provided more than 20 focal mechanisms for earthquakes showing a local magnitude ranging between $2 < M_l < 3.7$ and one $M_s = 5.6$ earthquake, located in and around the Marie-Galante graben. All focal mechanisms show nearly pure normal motion along sub-E–W-trending nodal planes, consistent with kinematics indicators observed along the Gosier and Morne Piton faults. This tectonic pattern is confirmed by GNSS velocities, which indicate that a small trench-parallel extension is accommodated in the upper-plate forearc (van Rijsingen et al., 2021).

Two historical earthquakes are reported along these two fault systems: (i) the 16 May 1851 earthquake with a maximum intensity of VII recorded in the southeastern part of Basse-Terre is attributed to the Morne Piton fault, with an estimated moment magnitude $M_w = 6.0$ (Feuillet et al., 2011), and (ii) the 29 April 1897 earthquake with a maximum intensity of VIII recorded in the Pointe-à-Pitre area is attributed either to the Gosier fault system, with an estimated moment magnitude $M_w = 5.5$, or to the Montserrat fault zone, with an estimated moment magnitude $M_w = 6.5$ (Bernard and Lambert, 1988; Feuillet et al., 2011). Overall, at the latitude of Guadeloupe, regional earthquake data suggest that normal fault systems are active and have an ability to generate earthquakes of moment magnitudes of M_w 6 and above. This magnitude range is potentially able to trigger tsunamis according

to tsunami catalogues (as explained, for example, in Roger et al., 2019).

4 Historical tsunamis

Southwest of the Marie-Galante basin, the 2004 M_w 6.3 earthquake (Bazin et al., 2010; Feuillet et al., 2011) showed that upper-plate crustal faults can generate strong earthquakes and tsunamis. The main shock occurred along the NNW–SSE-trending, ca. 40 km long arc-parallel Les Saintes fault System (Feuillet et al., 2011; Leclerc et al., 2016). The recurrence interval of such a rupture is estimated to be a few hundred years or more (Escartín et al., 2016, 2018; Feuillet et al., 2011; Le Friant et al., 2008). Focal mechanisms of the main shock and five aftershocks provided an overall pure normal motion along NNW–SSE nodal planes (Fig. 2d). Source models from Salichon et al. (2009), Bazin et al. (2010) and Feuillet et al. (2011), well constrained by the long duration of the aftershock sequence, proposed a main source localized along the N135° E-trending, 50° E-dipping Roseau fault (westernmost fault of the Les Saintes fault system), with a 30 km long and 21 km downdip width fault plane. The aftershock seismicity reactivated several nearby conjugate faults, with a maximum seismic depth at ca. 15 km. The main rupture occurred at two asperities located 8 km below the surface, with a maximum slip of 1.8 m, and propagated to the surface, triggering a coseismic offset of the seafloor of 0.3–0.6 m along a ca. 10 km long segment. Escartín et al. (2016) investigated the fault scarp by means of HR bathymetry, highlighting a 3 km long, up to 0.9 m high scarp, but concluded that part of the observed slip may be post-seismic. The Les Saintes earthquake generated up to 2 m high tsunami waves at the coast and a maximum horizontal run-up of 42 m in some bays of Les Saintes (Zahibo et al., 2005; Le Friant et al., 2008; Cordrie et al., 2020). However, tsunami models using fault parameters based on seismological data resulted in an underestimation of the tsunami wave amplitude and run-up (Le Friant et al., 2008). Cordrie et al. (2020) consider that their best-fit models require greater slip on the fault plane and a greater magnitude for the earthquake than those given by the seismological data in order to accurately reproduce the observed tsunami, suggesting that the observed scarp is the surface expression of coseismic slip (source parameters: $M_w = 6.4$–6.5; fault plane, 15×15 km; strike, N325° E; dip, 55° E; rake, ca. 90°; slip = 2.5–3.5 m).

Over the last ∼ 500 years of historical written archives in the Lesser Antilles, a few dozen confirmed tsunamis from different origins (local, regional or far-field sources including earthquakes, landslides, volcanic eruptions or combinations of them) have been reported. Starting with the 16 April 1690 $M_s \sim 8.0$ Barbados earthquake (which presumably triggered the first reported tsunami in the Lesser Antilles), it includes the widely studied 1 November 1755 Lisbon transoceanic tsunami (e.g., Gutscher et al., 2006; Accary and Roger, 2010; Roger et al., 2010, 2011; Martínez-Loriente et al., 2021) and the 18 November 1867 Virgin Islands tsunami (e.g., Zahibo et al., 2003, 2005; Barkan and ten Brink, 2010). Landslide sources or pyroclastic flows are also known for their tsunamigenic potential. In recent years, more and more studies have been carried out to assess the hazards associated with these "silent" tsunamis (e.g., Roger et al., 2024). In the Caribbean region, a few tsunamis triggered by landslides or pyroclastic flows have been reported in catalogues of events (e.g., O'loughlin and Lander, 2003; Accary and Roger, 2010), bathymetric surveys helped to identified large submarine landslide scars and deposits (e.g., Deplus et al., 2001; Le Friant et al., 2009, 2019), and a few studies have highlighted the capacity of these landslides to trigger large tsunamis (e.g., Smith and Shepherd, 1996; Teeuw et al., 2009; Leslie and Mann, 2016).

On the basis of an extensive literature review, including cross-checking of information, we conclude that only four tsunamis reported in Guadeloupe are likely of upper-crust seismic origin (Mallet, 1853, 1854, 1855; Lander, 1997; Zahibo and Pelinovsky, 2001; Lander et al., 2003; O'Loughlin and Lander, 2003; Zahibo et al., 2003; Accary and Roger, 2010; Nikolkina et al., 2010; Roger et al., 2013; online databases National Geophysical Data Center/World Data Service (NGDC/WDS), NOAA 2024, and Tsunami Laboratory/Institute of Computational Mathematics and Mathematical Geophysics (TL/ICMMG), 2023). These tsunamis have been observed or recorded following earthquakes occurring on regional faults (indicated magnitude and epicenter coordinates are from the USGS online earthquake catalogue: https://www.usgs.gov/programs/earthquake-hazards, last access: October 2022): the $M_w \sim 8.0$–8.5 earthquake on 8 February 1843 (NE of Guadeloupe, 16.73° N, 61.17° W) and the M_w 7.2 earthquake on 25 December 1969 (SE of Guadeloupe, 15.648° N, 59.694° W), which are arguably attributed either to a rupture along the megathrust or to upper-plate faulting; the M_w 6.5 earthquake on 16 March 1985 (along the Montserrat–Havers–Bouillante fault system between Montserrat and Nevis, north of Basse-Terre, 17.013° N, 62.448° W); and the M_w 6.3 earthquake on 21 November 2004 (along the Les Saintes fault system, south of Basse-Terre, 15.679° N, 61.706° W; Fig. 1). The largest earthquakes and tsunamis produced at subduction zones are expected to originate from rupture at the plate interface megathrust. However, historical records in the Lesser Antilles reveal that neither the 1843 M_w 7.5–8.5 nor the 1839 M_w 7.5–8.5 largest known earthquake, although destructive, has been followed by large tsunamis. However, Roger et al. (2013) showed that the simulation of a M_w 8.5 1843-like megathrust earthquake would have produced wave amplitudes of 5 m and more along the exposed coasts of Guadeloupe, which was not reported in coeval documents. Feuillet et al. (2011) explain that these two major earthquakes had a great rupture depth along the megathrust, consequently leading to slight seafloor deformation. However, numerical sim-

ulations of worst-case scenarios for these two ruptures along the megathrust evidence the possibilities of tsunami amplitudes up to 10 m and above in some embayment (Roger et al., 2013; Colon-Useche et al., 2023). As the magnitude of crustal earthquakes is constrained by the fault length, events occurring along such a crustal fault show a much smaller magnitude than megathrust earthquakes, which consequently may form smaller seafloor offsets. Thus, most crustal earthquakes that are able to trigger a tsunami do not produce significant sea surface deformation (only a few centimeters amplitude in most cases) compared to subduction interface earthquakes. Associated tsunamis are typically only visible on pressure gauge records (coastal gauges or DART systems) after processing the data (e.g., de-tiding and high-frequency filtering).

5 Material and method

5.1 Seismic lines

We present eight multichannel seismic (MCS) lines acquired during five oceanographic campaigns (location in Fig. 3a; uninterpreted profiles are provided as Supplement Figs. S1 and S2). These include high-resolution sparker source seismic data from KaShallow 1 (Lebrun et al., 2008) and GEOBERYX03 oceanographic campaigns (Thinon and Bitri, 2003; Thinon et al., 2004, 2010), mid-resolution GI airgun array seismic data from KaShallow 2 (Lebrun et al., 2008) and Aguadomar (Deplus et al., 1998) cruises, and deep-penetrating MCS data from the Sismantilles 1 seismic experiment (Hirn, 2001; Table 1).

Sismantilles 1 seismic data were processed using CGG Veritas Geovecteur® software on board the R/V *Nadir* (Hirn et al., 2001). Processing includes band pass filtering, internal and external mute, one-step velocity analysis, normal-moveout (NMO) correction, stack, predictive deconvolution, and post-stack constant water-velocity time migration. KaShallow 1 and 2, Aguadomar, and GEOBERYX03 were processed with Seismic Unix software (Cohen and Stockwell, Center for Wave Phenomena, Colorado School of Mines). The seismic processing includes band pass filtering, sea waves and spherical divergence corrections, constant velocity or simple velocity gradient NMO correction and stack, and constant water-velocity time migration. The reflection seismic lines are in millisecond two-way travel time (mstwt). The velocities of the wide-angle seismic (WAS) refraction profiles are in second two-way travel time (stwt).

5.2 Bathymetry

High-resolution bathymetric data were acquired during the KaShallow 2 oceanographic campaign (Lebrun, 2009) using a Simrad EM300 multibeam echo sounder. We merged these data with the Aguadomar (Deplus, 1998) and Sismantilles 2 (Laigle et al., 2007) cruise Simrad EM12 dual multibeam echo-sounder data available for the Marie-Galante basin. Vertical accuracy for these echo sounders is plurimetric for the typical water depth found in the Marie-Galante basin (< 2000 m below mean sea level, noted b.s.l. hereafter). Near-shore (0–200 m b.s.l.) and onshore, very high resolution bathymetric and topographic data come from the Litto3D database – https://www.geoportail.gouv.fr/donnees/litto3d (last access: 2 October 2022) – which includes airborne lidar survey and KaShallow 3 multibeam data acquired with a RESON SeaBat 8101 multibeam echo sounder. The vertical accuracy for this second dataset is better than 1 m. We used the Caraibes software (Ifremer) to process the data and to produce a 25 m grid spacing digital elevation model of the Marie-Galante basin and surrounding islands. Maps are produced using the open-access QGIS software (https://www.qgis.org, last access: August 2024).

5.3 Depth and time calibration of main geological boundaries

In order to measure offsets of unconformities on time-migrated seismic lines, we need to constrain the seismic velocities within the sediments. We used velocities from the WAS profile (Kopp et al., 2011) in the south of Marie-Galante that trends parallel to the MCS line Agua116 (Cornée et al., 2023). The WAS velocities in the ca. 0.4 stwt (second two-way time) thick upper unit (MG-MS3, Cornée et al., 2023) range between 2 and 2.5 km s^{-1}. The 3.25 km s^{-1} isochrones mimic the base of unit MG-MS2, and the 4.5 km s^{-1} isochrones follow the acoustic basement below MG-MS1. Moreover, KaShallow 2 cruise MCS data (Table 1) acquired with a 600 m long streamer allow us to determine the normal-moveout velocities down to a depth of ca. 0.75 stwt in well-layered units such as shown by the seismic lines (Fig. 3). Once converted into interval velocities using the Hewitt Dix formula, we determine velocities in the upper unit from 1500 to 2750 m s^{-1} (Dix, 1955). Therefore, we use 1500 m s^{-1} in the water and 2000 and 2500 m s^{-1} in the sediments to estimate (and bound) the depth of unconformities observed on time-migrated seismic lines (Table 2).

Offshore, several first-order unconformities and sedimentary units were accurately dated using biostratigraphy analysis or radiochronology (Bouysse and Mascle, 1994; KaShallow research program results, Münch et al., 2013; De Min et al., 2015; Cornée et al., 2023). The deepest dated unconformity, MG-SB2, which corresponds to the top of the MG-MS1 sequence, occurs on seismic lines east of Marie-Galante (thick orange line in Fig. 5, lines AGUA97, K09-09, K09-45 and Sis7C). Along the seismic line Agua97, the F8 fault scarp was sampled at 514 m b.s.l. just beneath the unconformity (KaShallow cruise ROV dive, Fig. 6). The samples BMG2 and BMG4 yielded a late Burdigalian/earliest Langhian age (Cornée et al., 2023). Thus, we propose 16 ± 1 Ma for the age of MG-SB2. Above, another regional unconformity, MG-SB3 (Cornée et al., 2023), is identified

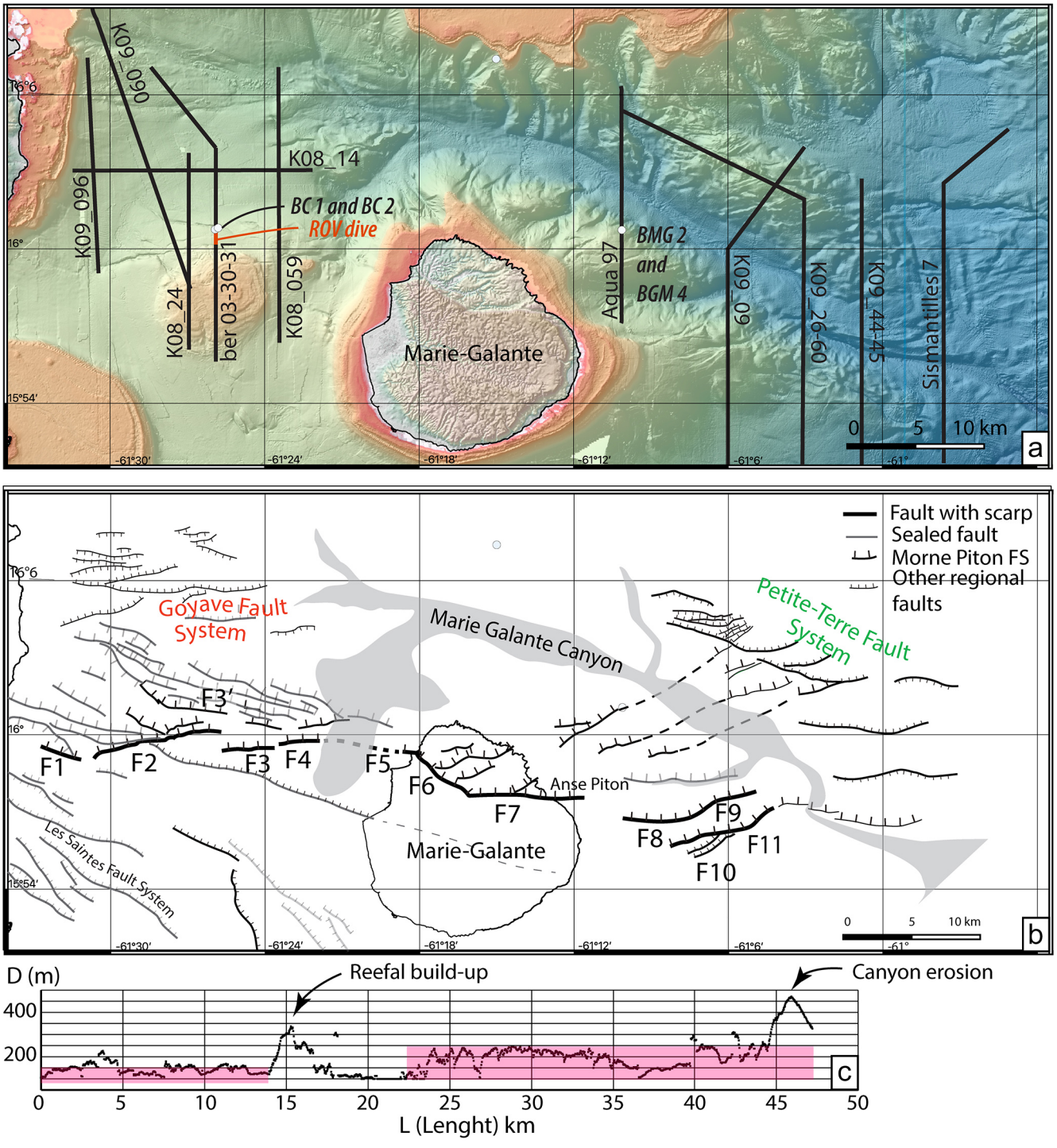

Figure 3. **(a)** High-resolution (25 m grid spacing) bathymetric map (UMO16) of the Marie-Galante basin, offshore Guadeloupe, and the location of the seismic profiles shown in Figs. 4 and 5, as well as the location of the dredge samples used for the seismic unit age calibration (Münch et al., 2013). **(b)** Structural interpretation of the E–W-trending Morne Piton fault system. **(c)** A proxy for cumulative strain given by the graphic displaying the fault surface displacement, taken as the difference between the top and the toe of the fault scarp versus L (fault length) along the whole system.

Table 1. Main acquisition parameters of the seismic data shown in this study (Figs. 4 and 5); CDP stands for common depth point.

Cruise	KaShallow 1	KaShallow 2	Aguadomar	Sismantilles	GEOBERYX03
Seismic source	1000 J sparker	35–45 in GI airgun array	45–105 in two GI airguns	4400 in airgun array	1000 J sparker
Peak frequency (far field)	250–400 Hz	40–70 Hz	30–50 Hz	15–20 Hz	250–400 Hz
Number of traces	6 traces	72 traces	6 traces	360 traces	6 traces
Fold coverage	3/6-fold	9/18-fold	3-fold	30-fold	3/6-fold
Inter-CDP distance	4 m	3.125 m	4 m	6.25 m	4 m

east of Marie-Galante. It corresponds to the top of the MG-MS2 sequence (thick purple line in Fig. 5, lines Agua97, K09-09-08, K09-45-44 and Sis7C). The age for this surface is bracketed between the late Messinian Grande-Terre (GT) carbonate platform (zones N18; 5.8–5.33 Ma; Cornée et al., 2023) and the sedimentary unit dated late Tortonian, 8.57 ± 0.43 Ma (Ar–Ar, Münch et al., 2014). We thus consider 7 ± 1.5 Ma for the age of MG-SB3. West of Marie-Galante, the angular unconformity on line K09-90 northwest of Marie-Galante may corresponds to MG-SB3 (Fig. 4). However, this reflector is too deep to be followed across the whole fault system. Within the uppermost sequence, MG-MS3, a remarkable unit boundary corresponding to a second-order unconformity can be easily correlated throughout the basin and onshore (thick red line in Fig. 4). This unit boundary is middle–late Piacenzian offshore, and it correlates with the 3–2.9 Ma tectonically induced erosional unconformity SB1 onshore (see above; Cornée et al., 2023). Along the seismic line Ber03-30-31, the fault scarp immediately north of F3 and F4 was sampled at 283 m b.s.l. (KaShallow cruise ROV dive, Fig. 4). Samples BC1 and BC2 yielded ages of 1.33 ± 0.23 Ma and 1.15 ± 0.12 Ma, respectively (Ar^{40} / Ar^{39} ages on plagioclases, Münch et al., 2013; 2014). These samples correspond to a prominent seismic reflector within the upper unit of the MG-MS3 sequence that can also be easily correlated through all the seismic lines west of Marie-Galante. We thus retain an average age of 1.29 ± 0.26 Ma for this seismic reflector (green line in Fig. 4).

5.4 Tsunami modeling

In order to test the tsunamigenic potential of the fault system proposed herein, a rupture scenario is elaborated on and is presented hereafter.

Numerical simulations of tsunami generation and propagation were carried out using COMCOT software (Cornell Multi-grid Coupled Tsunami, Liu et al., 1998; Wang, 2008; Wang and Power, 2011). COMCOT is widely used by the research community and constantly tested notably through various real tsunami cases (e.g., Prasetya et al., 2011; Gusman et al., 2019; Paris et al., 2021; Gusman et al., 2022; Roger et al., 2023). COMCOT uses a modified staggered finite-difference scheme to solve linear and non-linear shallow-water equations in either spherical or Cartesian coordinate systems throughout a set of nested grids, allowing refinement of the bathymetric resolution in coastal areas. A two-way nested grid configuration is implemented in the model to balance computational efficiency and numerical accuracy (Wang, 2008; Wang and Power, 2011).

For this study, nesting was used with two grid levels: the first grid is a 0.5 arcmin (~ 900 m) resolution grid of the Lesser Antilles (extent: 295° E, 302° E, 12° S, 18° S) built from the global dataset GEBCO 2021 (GEBCO Compilation Group, 2021); the second grid is a 3.75 arcsec (~ 115 m) spatial resolution grid focusing on the Guadeloupe archipelago and Dominica island, including the location of the investigated Morne Piton fault system as shown in Fig. 1 (extent: 297.92° E, 300.22° E, 14.94° N, 16.717° N). This second grid was built from different datasets including the aforementioned bathymetric data (Sect. 5.2). The highest-resolution and most recent data were kept first. Data gaps were filled in with data from GEBCO (GEBCO Compilation Group, 2021) for offshore regions and SRTM version 3.0 global 1 arcsec data (NASA SRTM, 2013) for onshore regions. Continuity of the different datasets was ensured using kriging interpolation, which has proven to be one of the best methods to produce a well-defined DEM, especially for smooth transitions between different resolution areas (e.g., Bernardes et al., 2006; Arun, 2013; Ajvazi and Czimber, 2019). Note that Dominica was included in the second grid in order to look at potential effects which could occur between the different islands and also to assess the potential tsunami threat resulting from the Morne Piton scenario on this neighboring island.

The initial sea-bottom displacement is calculated by COMCOT considering an instantaneous rupture of the fault using the surface deformation model of Okada (1985), and transmission of the deformation to the water column above is considered to be instantaneous. Calculations of wave propagation were done at mean sea level (MSL) assuming a constant Manning roughness coefficient of 0.011 for the seabed friction (Wang et al., 2017). A higher friction coefficient leads to more energy dissipation of tsunami waves, especially in shallow waters, slowing down their speed and reducing their amplitude and impact (e.g., Dao and Tkalich, 2007). Considering the limited extent of the interest zone (~ 250 km $\times$ 200 km), the rupture parameters (leading to a small coseismic rupture) and the objective to look at the potential localized effect as inter-island resonance, tsunami wave propagation time was set to 10 h.

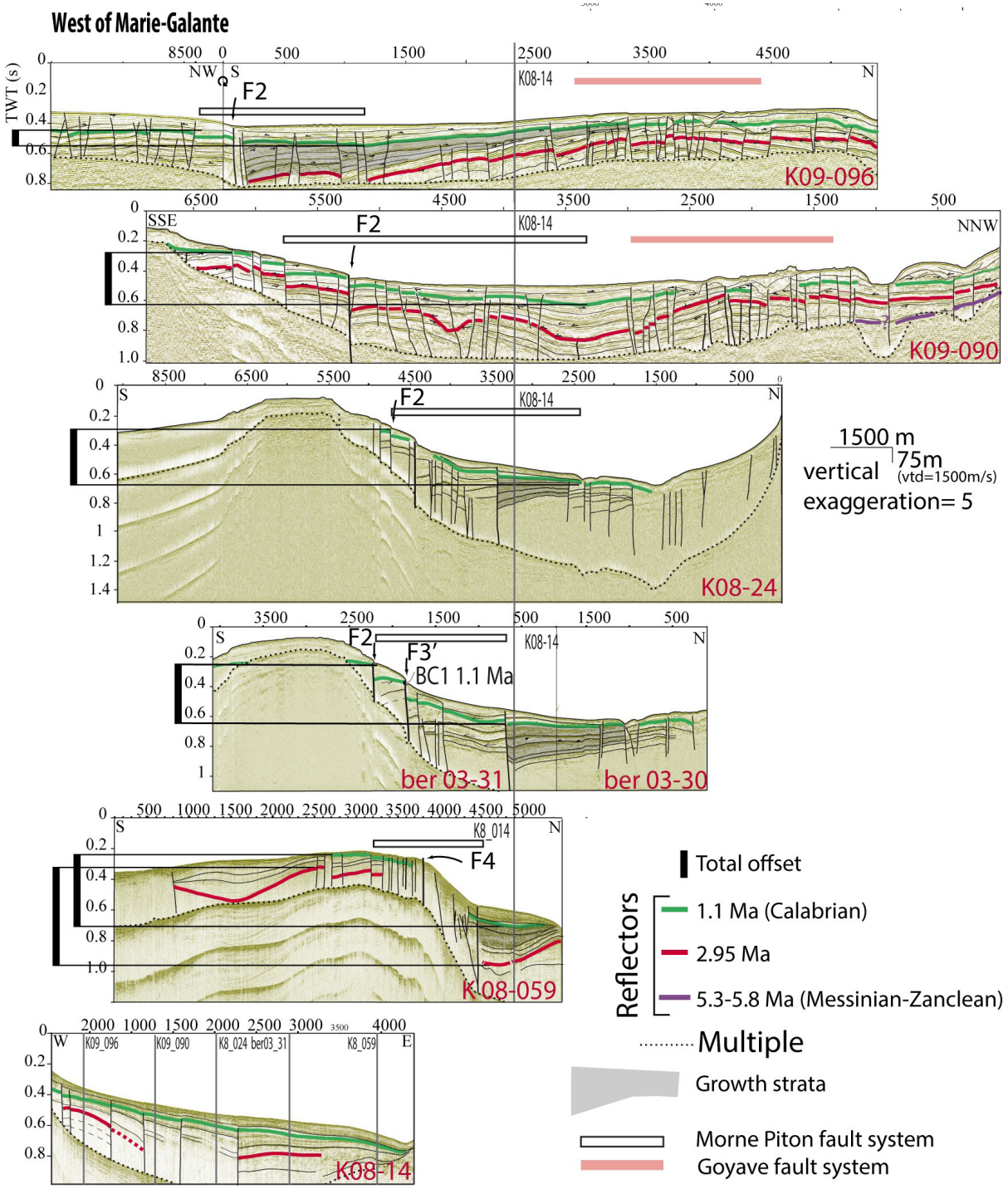

Figure 4. Seismic lines west of Marie-Galante (location in Fig. 3) showing the correlation across the Morne Piton fault system of the 1.29 Ma unit reflector (green) that corresponds to the reflector dredged at the BC1 and BC2 locations along the Ber03-30-31 seismic line. The 2.95 Ma unit boundary (red) is correlated with the seismic lines south of the Colombie bank and eastern Marie-Galante basin (line K09-90 and K09-26-62 location in Fig. 2). Notice that the basin sedimentary slope is in the E–W direction (parallel to line K08-14). Therefore, the initial topography of the reflectors in the N–S direction, across the fault system, can be neglected when measuring the offset along the seismic lines; uninterpreted profiles are provided in Supplement Fig. S1.

6 Results

6.1 The Morne Piton fault system

The HR bathymetric data presented in Sect. 5.2 allow us to refine the structural pattern of the Morne Piton fault system, especially offshore (Fig. 3a–b). The fault system splays eastward from the N120–N135° E-trending eastern Les Saintes fault system located east-southeast of Basse-Terre to the N110–115° E-trending Petite-Terre fault system south-southeast of Grande-Terre (Figs. 2 and 3). Thus, the fault zone spreads over a 5–8 km wide and 50 km long zone with an average N100° E trend.

Morpho-bathymetric analysis allows us to identify surficial segments of the faults that are reaching the seafloor. The main fault scarp of the Morne Piton fault system is the southernmost one, along which 11 fault segments of 1–10 km length can be identified (Fig. 3b). From west to east, the F1 segment trends N110° E and then the fault steps left along the N75° E-trending F2 segment. A little farther east, the fault cuts the northern Colombie bank and the eastern Marie-Galante platform along closely spaced N90° E-trending left or right stepping segments F3, F3', F4 and F5. Across the island, the F6 segment is a N130° E-trending, 6 km long right step relay linking the F5 segment to the F7 N90° E-trending one. Further east offshore Marie-Galante, four N80° E-trending fault segments, F8, F9, F10 and F11, are arranged as overlapping right steps. There, the fault scarp vanishes in just a few kilometers. To the east of line Sis7C, neither the sediments nor the basement is affected by the north-dipping Morne Piton fault system (Fig. 5). In contrast, the seismic line Sis7C shows that the basement is southwardly downthrown by the Petite-Terre fault system, along south-dipping active and sealed faults to the north and south of the Morne Piton fault system, respectively (Fig. 5 location in Fig. 3a). West of Marie-Galante, the Morne Piton fault system widens as closely spaced fault splays trending N95° E to N100° E link the main fault scarp (F2, F3 and F4) to the antithetic Goyave fault system or die westward (Fig. 4 location in Fig. 3a). Eastward of the F6 segment, some synthetic and a few antithetic faults splay northeastward and link with the N110–115° E Petite-Terre fault system.

The mean fault-scarp height west of Marie-Galante island is ca. 100 m (Fig. 3c). Across Marie-Galante island, the mean fault-scarp height reaches 200 m and controls the staircase morphology of the island. East of the island, the Marie-Galante canyon carved the sedimentary units, clearing some of the fault planes and increasing their apparent scarps heights up to 400 m. To the east, the canyon meanders and cuts through the eastern tip of the Morne Piton fault system (Fig. 3b and c). West of the island, in the vicinity of the volcanic island of Basse-Terre, either recent deposits or the uppermost sedimentary units seal most of the faults. These observations seem to indicate that the sedimentary rate west of

Table 2. Measured offset of seismic reflectors across the Morne Piton fault system and calculated total vertical strain rates. See text for the age estimate. Seismic reflector depth on each side of the fault system is measured in time (stwt, second two-way time) and converted into depth using water velocity (1500 m s^{-1}) and two end-member velocities for the sediment (see text for explanation), providing a minimum and a maximum offset value. The minimum strain rate is obtained from the ratio between the minimum offset and the maximum age bound of the reflector and vice versa.

Profile name sorted from east to west	Age (Ma)	Uncertainty (Ma)	Horizon depth in the footwall (stwt)		Horizon depth in the hanging wall (stwt)		V en m s^{-1} 2500 Horizon depth in the footwall (m)	V en m s^{-1} 2500 Horizon depth in the hanging wall (m)	V en m s^{-1} 2000 Horizon depth in the footwall (m)	V en m s^{-1} 2000 Horizon depth in the hanging wall (m)	V en m s^{-1} 2500 Total offset (m)	V en m s^{-1} 2000 Total offset (m)	Strain rate (mm yr^{-1})			Interval strain rate (mm yr^{-1})
			water	rock	water	rock	max	max	min	min	max	min	min	max	average	uncertainty
K09-44-45 – MG-SB2	16	1	1,575	0.83	1,575	1.22	2212.5	2700.0	2006.3	2396.3	487.5	390.0				
Since inception	7	1.5											0.046	0.089	0.067	0.030
K09-08-09 – MG-SB2	16	1	0.595	0.91	1.27	0.88	1577.5	2052.5	1351.3	1832.5	475.0	481.3				
Since inception	7	1.5											0.057	0.086	0.071	0.021
Agua97 – MG-SB2	16	1	0.05	0.72	1.36	0.6	937.5	1770.0	757.5	1620.0	832.5	862.5				
Since inception	7	1.5											0.101	0.151	0.126	0.035
K08-059 MG-UB4	2.95	0.05	0.23	0.09	0.59	0.37	285.0	905.0	262.5	812.5	620.0	550.0	0.183	0.214	0.199	0.022
K08-059	1.29	0.26	0.22	0.02	0.5	0.11	190.0	512.5	185.0	485.0	322.5	300.0	0.194	0.313	0.253	0.085
Ber03-31	1.29	0.26	0.21	0.04	0.53	0.1	207.5	522.5	197.5	497.5	315.0	300.0	0.194	0.306	0.250	0.079
K08-24	1.29	0.26	0.25	0.04	0.6	0.03	237.5	487.5	227.5	480.0	250.0	252.5	0.163	0.243	0.203	0.056
K09-090	1.29	0.26	0.33	0.02	0.49	0.13	272.5	530.0	267.5	497.5	257.5	230.0	0.148	0.250	0.199	0.072
K09-096	1.29	0.26	0.32	0.12	0.44	0.14	390.0	505.0	360.0	470.0	115.0	110.0	0.071	0.112	0.091	0.029

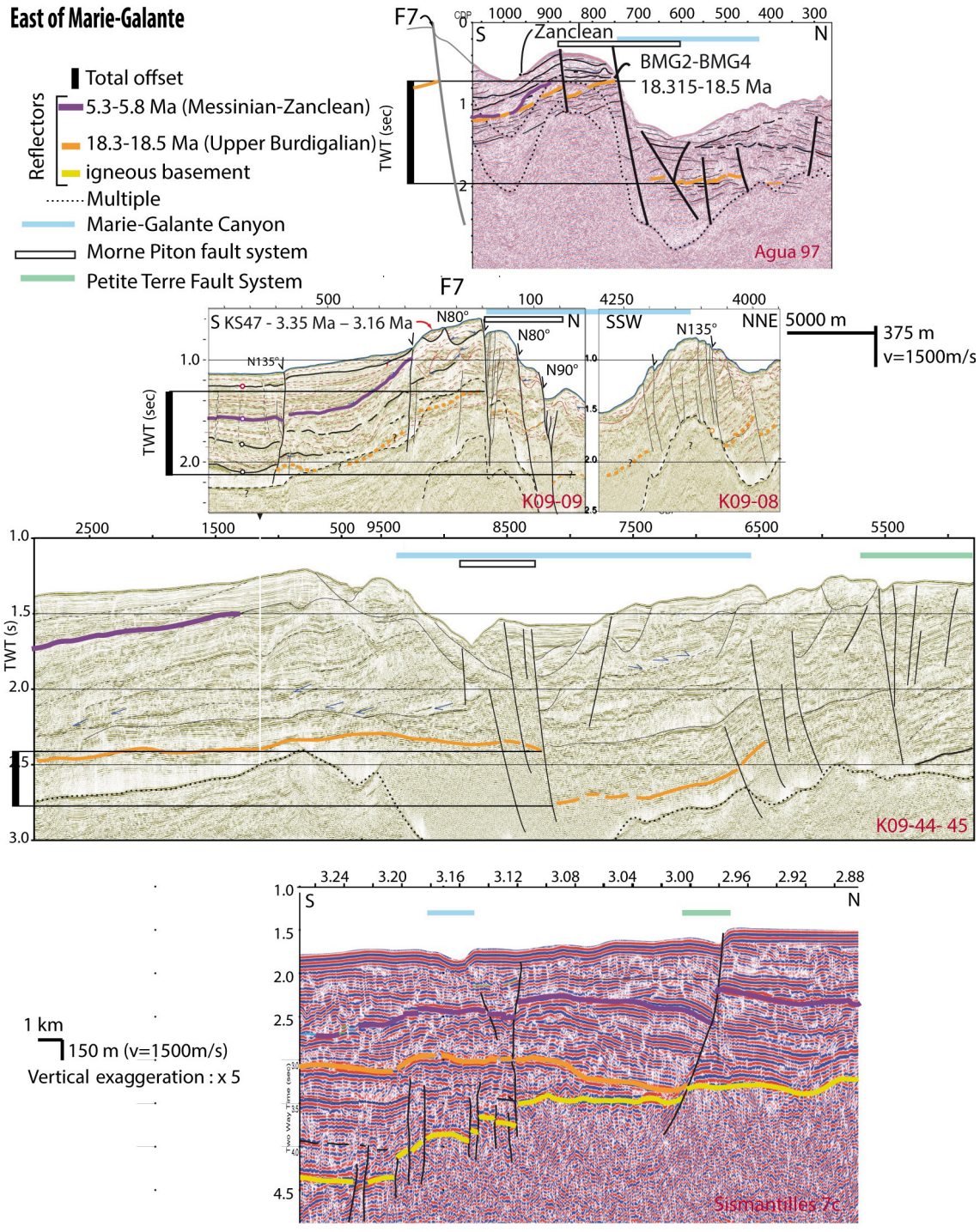

Figure 5. Seismic lines east of Marie-Galante illustrate the correlation across the Morne Piton fault system of the 7 Ma (Tortonian/Messinian) MG-SB3 sequence boundary (Purple) and the 16 Ma (Burdigalian) MG-SB2 sequence boundary (Orange). Seismic line location in Fig. 3; uninterpreted profiles are provided in Supplement Fig. S2.

Marie-Galante and the erosional rate east of Marie-Galante (in the canyon) exceed the vertical slip rate of the fault.

6.2 Vertical slip rate estimates along the Morne Piton fault system

To assess the average vertical slip rate along the Morne Piton fault system, we estimated the fault offset of key dated reflectors across the entire length of the fault system (Figs. 4 and 5; Table 2). West of Marie-Galante, the main offset of the 1.29 ± 0.26 Ma seismic reflector (green in Fig. 4) increases from west to east (i.e., from the westernmost extremity of the fault toward its center). Close to the eastern shore of Basse-Terre island (Fig. 4, profile K09-96, and Table 1), the 1.29 Ma reflector is downthrown by 110–115 m. Eastward, the reflector offset increases up to 230–257 m (Fig. 4, lines K09-90 and K08-24, and Table 2) and reaches a maximum of 300–322 m (Fig. 4, lines Ber03-30-31 and K08-59). Accordingly, the number of sealed structures across the fault system decreases eastward (Figs. 3 and 4). Thus, west of Marie-Galante, the Morne Piton fault system accommodates a vertical slip rate increasing eastward up to 0.25 ± 0.08 mm yr^{-1} over the last 1.29 ± 0.26 Myr (Table 2).

The 2.95 ± 0.05 Ma unit boundary (red line in Fig. 4) can only be correlated across the fault system along the K08-59 seismic line. Growth strata, characteristic of synsedimentary faulting, are observed in the deposits above the 2.95 Ma unit boundary (Fig. 4, gray shadow on seismic lines). This unit boundary offset reaches 550–620 m, leading to a 0.20 ± 0.02 mm yr^{-1} average vertical slip rate over the last 2.95 ± 0.05 Myr, i.e., ca. 0.16 mm yr^{-1} for the period 2.95–1.29 Ma (Table 2). West of Marie-Galante island, deeper reflectors cannot be identified and correlated across the fault system because of the limited seismic penetration.

However, east of Marie-Galante, the MG-SB2 sequence boundary dated to 16 ± 1 Ma (orange in Fig. 5; see also Fig. 5 in Cornée et al., 2023) is the only reflector that can be correlated on both sides of the fault system. In the hanging wall of the fault, the younger MG-SB3 7 ± 1.5 Ma boundary (Purple in Fig. 5) and a large part of the fault scarp are eroded by the Marie-Galante canyon. The seismic line K09-09 (Fig. 5) shows that the MG-SB3 unconformity records the Morne Piton fault inception: in the footwall of the fault, the stratigraphy of the MG-MS2 sequence (comprised between MG-SB2 and MG-SB3) shows conformal deposits flexed upward while approaching the fault, whereas MG-MS3 deposits onlap onto MG-SB3 and present clear growth strata. We thus propose that the 16 ± 1 Ma sequence boundary is pre-tectonic and is tilted by the fault since its inception at 7 ± 1.5 Ma (the age of MG-SB3; Fig. 5, profile K09-45-45). Along the fault system east of Marie-Galante, we calculated the strain rate from the MG-SB2 offset since 7 ± 1 Ma. From east to west, the slip rate ranges from 0.067 ± 0.03 mm yr^{-1} at the K09-44-45 seismic line to 0.071 ± 0.02 mm yr^{-1} along the K09-08-09 line. Seismic line Agua97 (Fig. 5) presents the greatest offset of MG-SB2. However, this seismic line does not cross the southernmost F7 segment (the water depth is too shallow for ship navigation in the footwall compartment). We estimated the depth of MG-SB2 in the footwall compartment from the closest seismic line available that crosses the fault located 1 km east of the Agua97 line. We obtain an offset of 830–860 m, leading to a maximum average vertical slip rate of 0.12 ± 0.03 mm yr^{-1} since 7 ± 1.5 Ma, i.e., ca. 0.07 mm yr^{-1} for the period 7–2.95 Ma (Table 2). Consequently, we propose (i) that the vertical slip rate accommodated by the Morne Piton fault system increases progressively from each extremity of the fault toward its center and (ii) that the Morne Piton fault system is characterized by an increasing slip rate from ca. 0.07 from its inception (i.e., 7 Ma) to ca. 0.25 mm yr^{-1} since 1.29 Ma (Table 2).

6.3 Earthquakes parameters of tsunami modeling

ROV dive along the Ber03-30-32 seismic line allowed observation of one of the main morphologic scarps of the Morne Piton fault system across the F2 and F3' segments (Figs. 3 and 6). Across the upper plateau, between F2 and F3', we observed several N90° E-trending fractures parallel to the fault segments (Fig. 6a). While descending across the F3' scarp, the slope progressively steepens up from 45° at 157 m b.s.l. to more than 80° at 280 m b.s.l., just a few meters above the toe of the scarp (Fig. 6a, b and c). This morphology suggests a ca. 128 m high cumulative scarp for the F3' segment at that location. The very last meter of the fault scarp above the toe of the slope presents a 100 cm high polished vertical surface, partly altered, showing dip-slip striations indicating pure normal motion along this fault segment (Fig. 5d e and f). This exposed and partly altered fault slip plane breaches the seafloor at a high angle. Such a polished striated fault-scarp morphology is similar to, although more altered compared to, the coseismic fault scarp observed at the toe of the Roseau fault plane after the Les Saintes earthquake (Escartín et al., 2016). We conclude that this observation of the Morne Piton polished striated scarp may correspond to one of the last coseismic scarps formed during a major earthquake (including possible post-seismic slip motion) along this fault. Alteration of the fault slip plane suggests that the slip event occurred tens to several hundreds of years ago; i.e., this fault slip plane may correspond to a pre-instrumental earthquake (see Discussion). From this observed scarp, we obtained a ratio of the last scarp event over total scarp height (a proxy for the cumulative slip as determined in Fig. 3) of ~ 2.6 %. With this ratio we calculated an average scarp of ~ 75 cm along the whole length of the fault and a maximum scarp of 2 m. Such an average scarp value corresponds to the surface expression of a magnitude $M_w \sim 6.7$ earthquake using the criteria of Wells and Coppersmith (1994) or even $M_w \sim 7$ according to Thingbaijam et al. (2017). The same studies also provide a calculated maximum displacement of ~ 2 m, consistent with the maximum observation along the scarp. Moreover, the 45 km

total length of the Morne Piton fault system measured from HR bathymetry, together with the width of the fault given by the 10 to 15 km thick seismogenic crust, leads to a rupture area ranging between ~ 450 and 675 km^2 that would generate a magnitude $M_w \sim 6.7 \pm 0.1$ earthquake, corroborating the aforementioned range of magnitude deduced with other observations (e.g., M_w ranging between 6.6 and 6.8 according Wells and Coppersmith, 1994, and Leonard, 2010, and around 7 according to Thingbaijam et al., 2017). The rupture parameters for the different identified segments of the fault shown in Fig. 3b are provided in Table 3. The geographic locations of the center of the top of the fault plane and azimuth are provided based on our structural analysis (Sect. 6.1 and 6.3). Neither seismic lines which illustrate only a few hundred meters nor in-depth earthquake distributions (which are not resolved enough) allow us to estimate the dip of the Morne Piton fault system. Thus, after considering the influence of the dip on surface deformation, which turns out to be negligible, we choose a mean dip of 75° for the fault segments after Feuillet et al. (2004). The shape of the rupture area (along-strike length × downdip width) and a slip of 1.89 m (maximum displacement estimated from scarp height measurement) is implemented for each segment in order to fit with a total fault surface of ca. 500 km^2, corresponding to a magnitude M_w 6.5 earthquake. Finally, in accordance with pure dip-slip striations observed along the F3' segment during the ROV dive (Fig. 6e), we apply a rake of 90°, corresponding to pure normal faulting. This is consistent with observations of dip-slip kinematic criteria made (i) along the F7 segment by Feuillet et al. (2002) and (ii) onshore at Anse Piton (Marie-Galante) by Feuillet et al. (2004). Fault segments F8 and F9 are not straight, and for the purpose of modeling they are divided into F8–F9 and F10–F11 (Fig. 7). Hereafter, we use these parameters to evaluate the potential tsunami hazard from the Morne Piton fault for a worst-case plausible scenario rupturing all the segments simultaneously.

6.4 Plausible worst-case tsunami scenario and resulting hazard

We present a worst-case plausible scenario, related to a rupture along all the identified segments of the Morne Piton fault system as these 1 to 10 km long segments most probably root in depth along a single fault zone (Feuillet et al., 2004). We rule out the eventuality of testing a single 10 km long segment of the Morne Piton fault system rupture as it would generate a $M_w < 6.0$ earthquake and would thus unlikely consist of a tsunami source (e.g., Roger et al., 2019). Here, we use a plausible M_w 6.5 scenario, i.e., a magnitude slightly lower that the maximum magnitude M_w 6.7 deduced from the morphological analysis but close enough to the Les Saintes earthquake magnitude as both the Les Saintes and Morne Piton fault systems share close morphological characteristics. Our model would generate a tsunami with significant energy/amplitude to accurately highlight the potential consequences of tsunami waves' propagation and interaction with the peculiar shallow reliefs and major embayment located in and around the Marie-Galante basin. Quantifying horizontal run-up at the coast and assessing tsunami risk following a rupture along this fault is out of the scope of the present study, as such quantifications necessitate a better understanding of the fault dynamic itself (e.g., return period of large events).

The initial surface elevation directly resulting from the Okada's (1985) formulation is presented in Fig. 7. Due to the high inclination of the fault planes (dip = 75°) dipping globally northward, a profile cut of the initial displacement is represented from the north to the south by a crest (positive elevation) and a trough (negative elevation). At t=0, the shallow-water equations take over from this initial deformation, and the propagation of the tsunami waves is calculated over the nested grids at adequate time steps. Figure 8 presents the state of the virtual water surface at six different times of the tsunami wave propagation from 1 to 16 min. The wave front initially parallel to the fault axes ($t \leq 1$ min) is progressively influenced by the bathymetry within the very first minutes following the rupture, leading to an anisotropic propagation of the waves showing variability in space and time. In addition, the fact that the fault literally crosses Marie-Galante leads to the tsunami source being divided into two independent sources located in the west and east of this island: two tsunamis are therefore generated and called TsuW (in the west) and TsuE (in the east) hereafter. These two tsunamis propagate from their origin and wrap around Marie-Galante as shown at $t = 4$ min of propagation. Then, between 4 and 9 min, the two tsunami fronts meet on the north and south of Marie-Galante. Meanwhile, the propagation of the TsuW waves meets the shallow waters of the Colombie bank shoal (approx. coordinates: 15.98° N, −61.43° W; minimum water depth is about 35 m) west of Marie-Galante: the waves' amplitude increases as they slow down, and their interaction leads to a constructive interference resulting in a new tsunami source at the Colombie bank shoal, mainly showing a negative wave propagating southward with some extensions toward Marie-Galante in the east and Les Saintes in the west.

Approaching the coasts, wave shoaling takes over, with the reduction in water depth slowing down the waves and simultaneously increasing their amplitude. It leads to wave amplification as particularly shown along the Marie-Galante north shore, the southeast coast of Basse-Terre, and the south of Petite-Terre and eastern Grande-Terre (Fig. 9).

After 10 h of tsunami propagation, the maximum values of wave amplitude reached on each point of the simulation domain are shown in Fig. 9. The overall impact of such an event is that the maximum wave amplitude is not going over 1.2 m, carefully considering the 100 m resolution of the simulation domain: in fact, grid refinement at the coast showing higher resolution would probably highlight higher wave amplitude in very localized areas because of interaction with small underwater structures not represented at this resolution, as well

Table 3. Parameters used for the tsunami source simulation of a rupture along the multi-segment fault presented in Fig. 7.

Fault segment	Longitude (°)	Latitude (°)	Length (m)	Width (m)	Top of the fault plane depth (m)	Strike (°)	Dip (°)	Rake (°)	Slip (m)
F1	−61.5335	15.98987	2838	12 500	500	111	75	−90	1.89
F2	−61.4708	15.994	9070	12 500	500	78	75	−90	1.89
F3’	−61.4428	16.01503	3918	12 500	500	95	75	−90	1.89
F3	−61.4108	15.99009	3474	12 500	500	88	75	−90	1.89
F4	−61.377	15.99367	2735	12 500	500	84	75	−90	1.89
F5	−61.3287	15.99021	6623	12 500	500	97	75	−90	1.89
F6	−61.2846	15.97275	4813	12 500	500	128	75	−90	1.89
F7	−61.2301	15.95767	7904	12 500	500	92	75	−90	1.89
F8	−61.1477	15.94221	4052	12 500	500	92	75	−90	1.89
F9	−61.1042	15.94958	5495	12 500	500	70	75	−90	1.89
F10	−61.111	15.93014	5336	12 500	500	78	75	−90	1.89
F11	−61.0777	15.94126	2228	12 500	500	52	75	−90	1.89

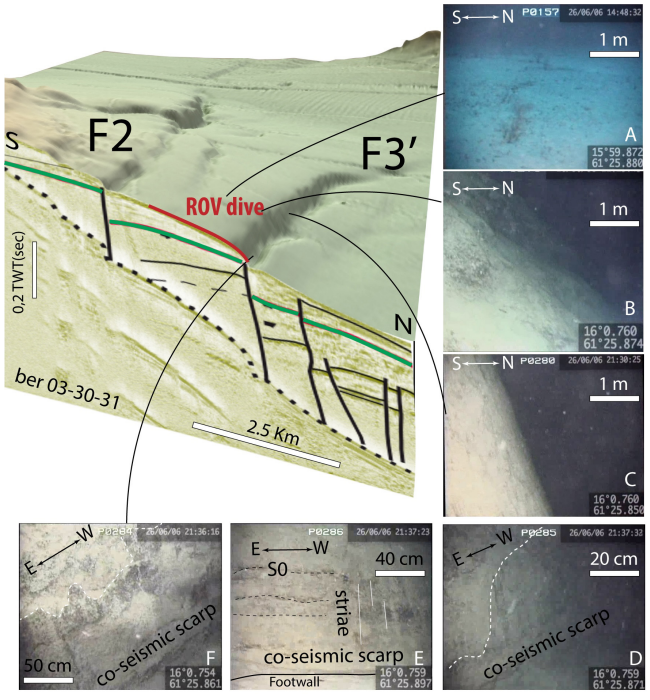

Figure 6. ROV photographs of the fault identified on the seafloor along the Ber03-30-31 seismic line across the F3’ Morne Piton fault segment (location in Fig. 3). **(a)** Photography of the hanging wall of F3’. The eroded F3’ fault plane presents a progressive downward slope steepening **(b, c)** until the toe of the fault, which is marked by a characteristic coseismic scarp with dip-slip striae **(d, e, f)**. In each panel, white numbers starting with a P represent the water depth in meters, latitude is north and longitude is west (WGS84). Panels **(a)**, **(b)** and **(c)** show areas several tens of square meters wide; panels **(d)**, **(e)** and **(f)** are close-ups showing a ca. 1 m high escarpment just above the foot of the fault scarp (visible at the bottom of each panel).

as non-linear effects. The patterns of those amplitudes indicate that not only the fault region but also some coastal regions are exposed to tsunami waves of 50 cm or more, which is above the usual beach and marine threat 30 cm threshold. It is the case for the neighboring coasts of Marie-Galante, southeast Basse-Terre, south Grande-Terre and the natural reserve of Petite-Terre. The southeast coast of Basse-Terre is particularly exposed, with wave amplitudes of more than 1 m (Fig. 9a). A focus on the Les Saintes archipelago also highlights wave amplitudes of more than 1 m, even between the islands (Fig. 9b). The northeast coast of Dominica is also affected but to a lesser extent (maximum wave amplitudes of $\sim$ 50 cm). Further high-resolution simulation, including flow speed calculations, would help to correctly assess the related hazard on this island. Virtual sea-level gauges were added at different locations of grid 2 (Fig. 9) in order to check if the model is stable and to look for possible resonance (especially in the Les Saintes archipelago). The raw signal of seven VG (top Fig. 10) highlights a clear decrease in the amplitude over time in all stations. However, for stations VG_1, VG_2 and VG_3, a low-frequency oscillation is clearly visible and lasts for at least 10 h. The amplitude spectrums on these three stations show that two peaks with a period of $\sim$ 8.5 and 15 min, respectively, are present on the three signals at Les Saintes, which is not the case for the stations out of the archipelago. Moreover, the high-amplitude negative wave southwardly propagating, generated by the new tsunami source at the Colombie bank shoal, is shown by VG_1 in Fig. 10, with a peak-to-trough value of $\sim$ 0.6 m. VG_2 and VG_3 also show it to a lesser extent a bit later.

7 Discussion

7.1 Upper-plate fault tsunamigenic potential

The Les Saintes earthquake demonstrated that upper-plate normal faults may generate $M_w > 6$ tsunamigenic earth-

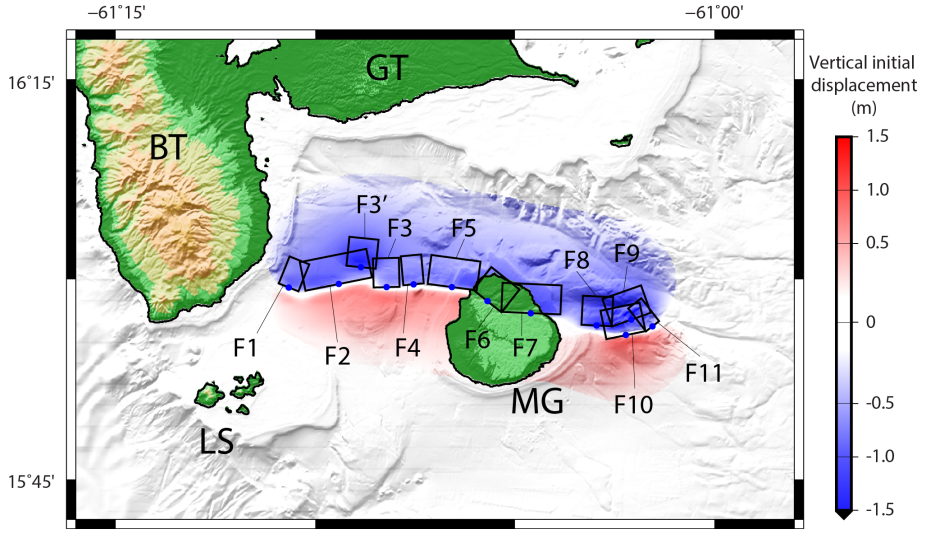

Figure 7. Initial surface elevation for a maximum credible scenario built with the 11 fault segments detailed in Table 3. Blue dots indicate the top fault center. Acronyms stand for Grande-Terre (GT), Basse-Terre (BT), Les Saintes (LS) and Marie-Galante (MG).

quakes in the Lesser Antilles. The Les Saintes tsunami produced up to 2 m high waves at the coast and 42 m distance run-up in a peculiar embayment (Zahibo et al., 2005). Such normal faults are prone to be tsunamigenic because their rupture is relatively shallow (compared to the megathrust), and their slip motion is favorable to large seafloor displacement. Together with their proximity to the islands, they are able to produce meter-high tsunami waves at the coast and tens to hundreds of meters of run-up distances (depending on the topography). Therefore, upper-plate crustal faults may represent a major potential tsunami hazard in the Lesser Antilles islands and particularly in the Guadeloupe archipelago as pointed out by the Intergovernmental Oceanographic Commission held in Fort-de-France in 2019 (IOC-UNESCO, 2020). Similarly to the Les Saintes fault, we assume that the 50 km long Morne Piton fault poses a potential earthquake and tsunami hazard. The large scarp we observed at the toe of the Morne Piton fault suggests a recent seismogenic rupture(s) along this structure, which is potentially tsunamigenic. However, this scarp might not be related to the 1851 historical event as the estimated magnitude M_w 5–5.5 for this earthquake appears too low to explain the observed scarp. Thus, a rupture of the fault along its whole length must not be excluded. Several other prominent onshore–offshore faults affect the seafloor and the topography of the archipelago and may represent both an earthquake and a tsunami hazard. However, the relationships between faults, earthquakes and tsunami is not clearly established as shown in the following examples.

Along the arc, the Montserrat–Havers–Bouillante and Les Saintes fault systems are the most prominent tectonic features (Feuillet et al., 2010). To the south, Les Saintes fault system dips east and defines a half graben (Leclerc et al., 2016). The westernmost fault, the Roseau fault, ruptured during the 2004 M_w 6.3 earthquake and is most likely reloading stress and therefore quiet. The recurrence time for this earthquake was estimated to be more than 1000 years given the slow regional strain rate. However, the eastern normal faults of the system offset the seafloor over more than 30 km and present tilted blocks filled by fan-shaped Late Pleistocene deposits showing recent deformation. In the light of these observations, the eventuality of a tsunamigenic earthquake along these faults should be considered. To the northwest along the Havers segment, a rupture occurred in 1985, with a M_w 6.5 earthquake showing strike-slip mechanisms. Beck et al. (2012) estimated a recurrence time of 6500–7000 years for such a M_w 6.5 event based on the vertical offset of coseismic deposits in hemipelagites imaged by very high resolution seismic lines across the fault. In between these two segments, the Montserrat–Bouillante segment is seismically quiet except if the 1897 (estimated M_w 7.0) earthquake occurred along this fault (Feuillet et al., 2011). However, no tsunami related to such a rupture has been reported. Seismic lines across the Montserrat–Bouillante fault (Feuillet et al., 2010; Legendre, 2018) reveal that the fault offsets the most recent units, including the oldest reflector drilled during the IODP1395 that dates to the upper Gelasian ca. 1.8–2 Ma (Le Friant et al., 2013). Given an offset of 0.3 m stwt and a 2000–2500 m s^{-1} sediment velocity, this provides a 0.15–0.2 mm yr^{-1} slip rate. Thus, the Montserrat–Bouillante segment should also be considered tsunamigenic (Fig. 2).

South of Grande-Terre of Guadeloupe, the N90° E-trending Gosier fault system bounds 45 km of coastal area (Fig. 2). The fault system offset the Middle Pleistocene Grande-Terre plateau that culminates at +150 m from the offshore plateau that rests 15–20 m b.s.l. (Münch et al.,

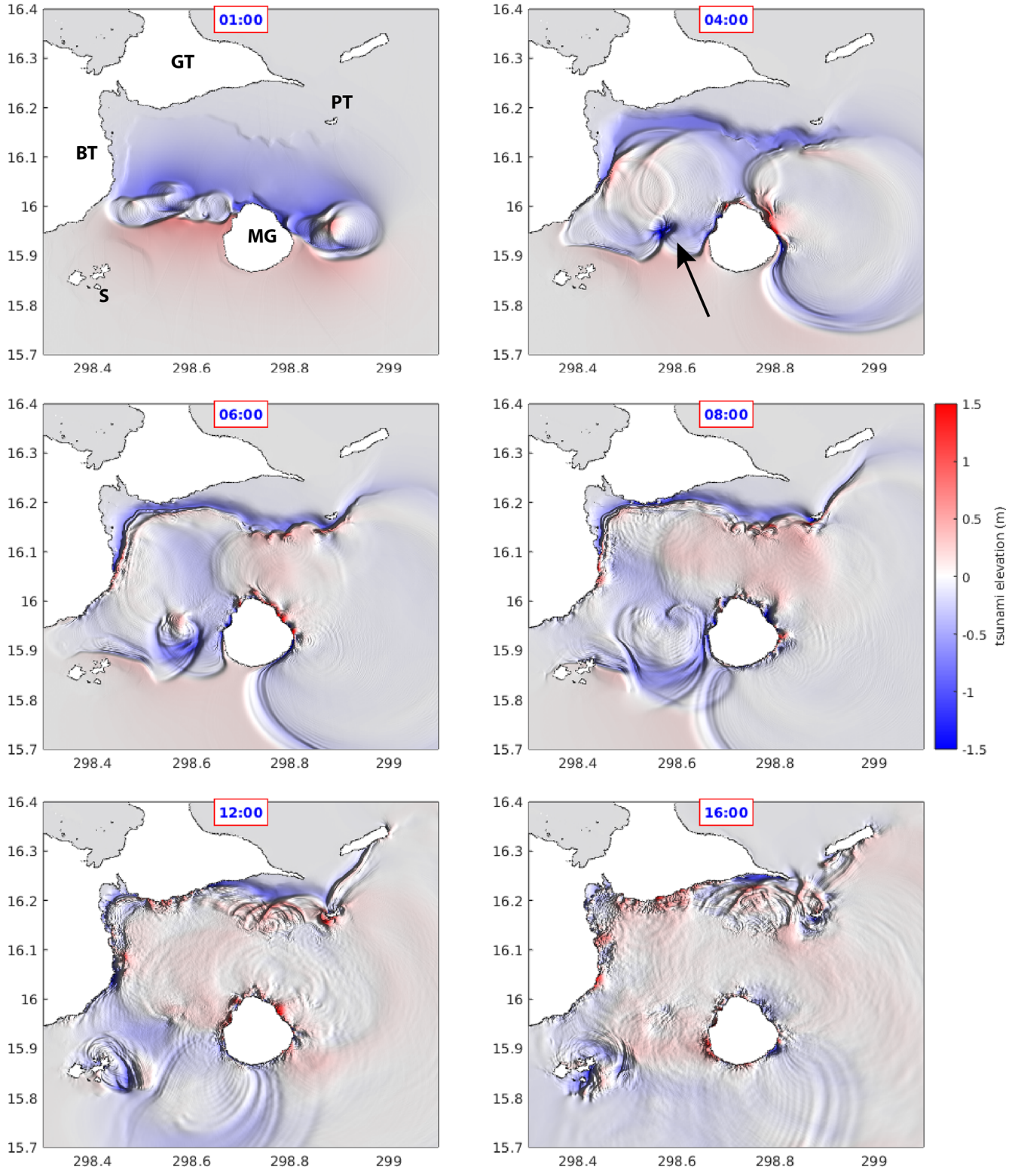

Figure 8. Snapshots of tsunami elevation within the Guadeloupe archipelago at 1, 4, 8, 6, 12 and 16 min of wave propagation. Red and blue colors correspond to wave crests and troughs, respectively. The black arrow shows the Colombie bank shoal. BT: Basse-Terre; GT: Grande-Terre; S: Les Saintes; PT: Petite-Terre; MG: Marie-Galante.

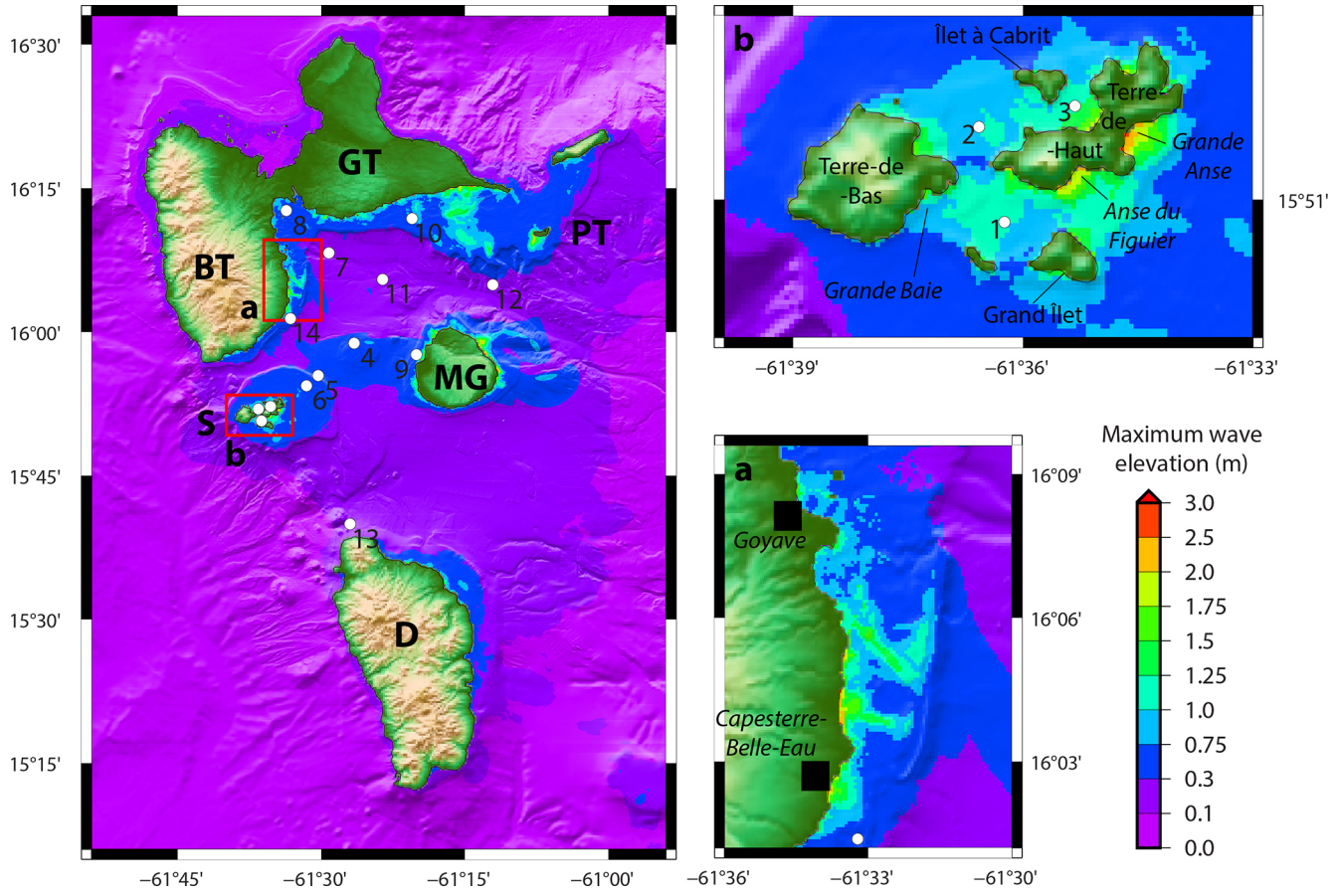

Figure 9. Shadowed bathymetric map with tsunami maximum wave elevation. Numbered white dots: 14 virtual sea-level gauges (VG); BT: Basse-Terre; GT: Grande-Terre; S: Les Saintes; PT: Petite-Terre; MG: Marie-Galante; D: Dominica. VG_4 and VG_11 are located near the fault rupture region, and VG_5 and VG_6 are near the Les Saintes fault system. VG_1, VG_2 and VG_3 are within the Les Saintes archipelago.

2013). This suggests a long-term vertical slip rate of ca. 0.10 mm yr^{-1}. To the east of Grande-Terre, the fault crosscuts the MIS5e terrace, showing the Late Pleistocene activity of the fault. However, evaluation of paleo-seismicity along one eastern segment of the fault system by means of trenches allowed the identification of recent surface ruptures, although superficial deposits remain undated (Terrier et al., 2002).

East of Guadeloupe, offshore, the Marie-Galante basin is bounded to the east by the Karukera spur (Fig. 2d), a 75 km long N–S-trending submerged plateau that culminates 30 m b.s.l. to the north offshore La Désirade island and gently dips southward down to ca. 1500 m b.s.l. (De Min et al., 2015). The spur is bounded to the west by N150° to N0° E-trending, west-dipping and normal faults. These faults offset the Middle Miocene sequence boundary (SB2) by up to ca. 2700–2900 m, leading to a long-term vertical slip rate of 0.16–0.18 mm yr^{-1}. Recent deposits are clearly affected by tectonic activity (Seibert et al., 2020). Located far from the islands, the earthquake intensity felt onshore would be relatively low in the island, but a tsunami could propagate across the Marie-Galante basin directly toward the coasts of the Lesser Antilles arc islands.

7.2 Slip rate reassessment along the Morne Piton fault system

With this study, we evidence that the slip rate along the Morne Piton fault system increases through time with a maximum slip rate of $0.25 \pm 0{,}08$ mm yr^{-1} over the last 1.29 Myr. This slip rate is up to 4 times slower than previous estimates. Over the last 330 kyr, Feuillet et al. (2004) estimate a bulk slip rate along the Morne Piton fault as high as 1 mm yr^{-1} over 330–125 ka and then decreasing to 0.3 mm yr^{-1} over the last 125 kyr. This last value is close to the long-term slip rate obtained offshore in this study (Fig. 11). These results suggest that the fault may present a fast slip rate during short periods of time (a few hundred kiloyears) separated by long periods (million years) of low slip rate. The fast 1 mm yr^{-1} rate was obtained considering that the terrace T2MG is offset by the fault by 159 m and dates to MIS7e (249 ka), and the

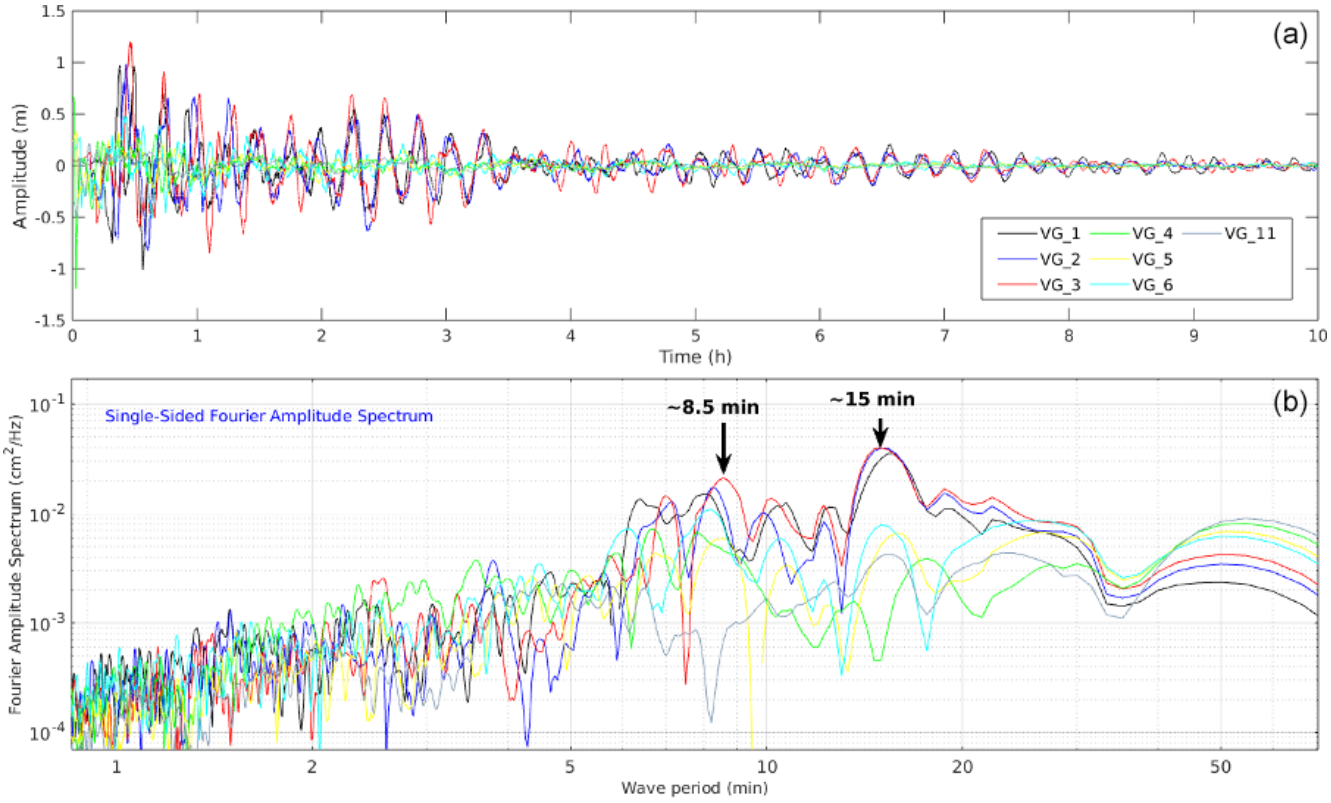

Figure 10. Post-processing of virtual gauge records. Top: sea-level records at seven different locations (VG_1 to VG_6 and VG_11; location in Fig. 9); bottom: single-sided Fourier amplitude spectrum. The black arrows symbolize the location of the two peaks with periods ∼ 8.5 and 15 min.

upper plateau of Marie-Galante corresponds to an abrasion surface from the MIS9e high stand (330 ka; Feuillet et al., 2004).

This latter statement can be reconsidered. The same *Agaricia* sp. limestone unit and *Acropora* sp. limestone unit top the three islands, Grande-Terre, La Désirade and Marie-Galante, suggesting they emerged synchronously (Feuillet et al., 2002; Cornée et al., 2012; Münch et al., 2013). In the three islands, the youngest formation, the *Acropora* unit, is not younger than 1.07 Ma and not older than 1.54 Ma (Cornée et al., 2012; Münch et al., 2014). From the geological map of Bouysse et al. (1993), this unit rims the Marie-Galante island. In La Désirade, the upper-plateau culminates at 276 m a.s.l. (above sea level), whereas the 330 ka terrace is at 35 m a.s.l. (Lardeaux et al., 2013; Leticée et al., 2019). Consequently, the hypothesis stating that the plateau emerged at 330 ka can be ruled out in Marie-Galante. Based on the age of the latest deposit of the Marie-Galante plateau that ranges between 1.54 and 1.07 Ma, a vertical slip rate of 0.15–0.22 mm yr^{-1} can be calculated. This value is close to the ca. 0.25 mm yr^{-1} obtained offshore for the slip rate along the Morne Piton fault system over the same period of time (Fig. 11). As a consequence, it is not possible to conclude that the Morne Piton fault system has short periods of a fast slip rate, but instead it probably increases through time, reaching a maximum slip rate of 0.25 mm yr^{-1} over the last million years. As a consequence, dividing the slip rate along the Morne Piton fault system by four increases the earthquake time recurrence along this fault system and thus the time recurrence of potential associated tsunamis. Constraining the fault slip rate at the timescale of one seismic cycle or a few seismic cycles may allow for better estimates of seismic and tsunamigenic hazards of the Morne Piton fault system. This would require a better understanding of in-depth fault geometry and identification of its active segments, which could be obtained by means of a microseismic survey (using ocean-bottom-seismometer acquisition over 1–2 years or more). In the present day, BOTDR (Brillouin Optical Time Domain Reflectometry) laser reflectometry is used to perform long-term monitoring of the Morne Piton fault using the network of submarine telecom fiber optic cables connecting Marie-Galante to the larger islands of Basse-Terre and Grande-Terre (Gutscher et al., 2023). It should be noted that given the slow strain rate and in the absence of rupture occurring along the fault during the survey period, identifying the slip rate across this fault system may require hundreds to thousands of years. Moreover, very high resolution seismic data across the fault in areas of high sedimentation rates (i.e., along the eastern

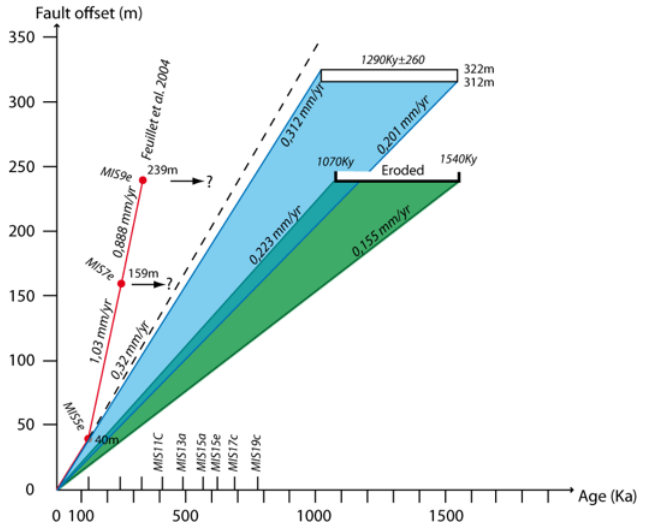

Figure 11. Fault offset along the Morne Piton fault against the age of the strain marker. Red: data from Feuillet et al. (2004) based on absolute age of terrace T4 (MIS5e), the estimated age of terrace T2 (MIS7e) and the suggested age of the Marie-Galante upper plateau (MIS9e). Green: strain range calculated using the upper-plateau unit age from Münch et al. (2014) (note that erosion may lower this estimation strain rate). Blue: strain range calculated from the fault offset of the seismic unit dated ca. 1.2 Ma along the seismic line K08-59 (green reflector in Fig. 4). The dotted line indicates the 0.32 mm yr^{-1} strain rate from the estimated offset of the MIS5e terrace in Marie-Galante (Feuillet et al., 2004).

coast of Basse-Terre island) may constrain the Holocene fault activity. Slip rate estimates can be obtained by coring and dating of (i) the most recent deformed sediments as well as (ii) tsunami deposits in salt marshes. Finally, such regional monitoring would also contribute to a survey of past and potential landslides that may also be induced by earthquakes and which may locally generate destructive waves.

7.3 Bathymetric feature control of tsunami wave propagation

The aim of the tsunami simulation associated with the present study is not to produce a precise hazard assessment for the islands of Guadeloupe but rather to give an overview of what could happen in terms of tsunami generation if all the identified segments of the Morne Piton fault system ruptured together and to identify a few gaps in terms of scientific knowledge and operational activities. An accurate hazard assessment study would require many rupture scenarios, including combinations of the segments used in this study, with variations in their parameters and sensitivity tests.

The main outcome of the simulation presented above lies in the fact that submarine features play an important role in the tsunami wave behavior and amplitude. Submarine canyons are known to focus the waves (e.g., along the continental slope of the middle American trench, Álvarez-Gómez et al., 2012; or at Nazarè, Portugal, Martins et al., 2010; do Carmo et al., 2022; Delpey et al., 2021). This behavior also occurs along the rim of the island submarine plateau, raising the wave amplitude as exemplified in front of the most populated cities of southeastern Grande-Terre (Fig. 9). Shallow-water plateaus located around or between islands slow down the waves, which leads to particular propagation patterns like the wrapping around the relief (Fig. 8). There, the wrapping effect of the waves around Marie-Galante and the Colombie bank result in two distinct tsunami sources, i.e., a primary source at the fault and a secondary one at the Colombie bank (Fig. 8). Such a behavior, already shown in other regions, is able to considerably amplify the impact of the tsunami on the coast opposite to the fault rupture (Chadha et al., 2005; Chen et al., 2012). It is important to notice that the low resolution of the grid used for the present simulations is a limiting factor in quantifying correctly the wave amplitude along the shoreline. A higher-resolution simulation grid would better reproduce the bathymetric features, especially in shallow waters, having a non-negligible impact on the waves' behavior and amplitude.

Our simulation also highlights interesting phenomena that would require further consideration in the framework of further tsunami hazard studies: wave oscillation, which could be attributed to a resonance effect, is clearly visible within the Les Saintes archipelago, and potential wave trapping is also visible around those islands. If the second case is purely observation, the resonance between the Les Saintes islands is clearly revealed by the single-sided Fourier amplitude spectrum (Fig. 10), and the peak at $\sim$ 15 min seems to be associated with the negative wave coming after the initial wave front and related to the tsunami interaction with the Colombie bank shoal. The records provided by the virtual gauges located beforehand within the archipelago (VG_1, VG_2 and VG_3) clearly show a long-period oscillation of the signal which is not present on the gauges located outside of Les Saintes (VG_4, VG_5, VG_6 and VG_11). It shows how the frequency content of the incoming signal can affect the sea level for many hours after the seismic rupture.

The numerical simulations performed by Cordrie et al. (2020) of the tsunami following the M_w 6.3 Les Saintes earthquake were able to match the witnesses' observations in Les Saintes (Zahibo et al., 2005). Despite the low resolution (100 m) of the present simulation on Les Saintes, there are some similarities between the two studies of potential impacted zones, for example, in the Marigot or Grande-Anse bays. It also shows that other bays, like the ones located between Terre-de-Haut and Îlet à Cabrit, appear to be quite well protected and are not exposed to relatively strong tsunami waves.

Finally, this study also highlights the exposed coastline of Dominica: on the north-northeast coast of the island (Fig. 9), 50+ cm waves are simulated, showing that this island should integrate such a scenario of crustal fault rupture within its tsunami hazard assessment plan.

8 Conclusions

Thanks to HR bathymetry, reflection seismic data and sediment samples, the analyses of the morphology and tectonic structures of the Marie-Galante basin located in the middle of the Guadeloupe archipelago allow us to detail the structural pattern of this region and to estimate a slip rate of ca. 0.1 mm yr^{-1} increasing over the last million years to 0.25 mm yr^{-1}, along the Morne Piton fault system, crosscutting the basin. This estimate divides the previously published estimations of the slip rate by four and thus increases the earthquake recurrence time associated with the Morne Piton fault system from 1 to 4–5 kyr. We show that a seismic rupture associated with an earthquake showing a moment magnitude $M_w \sim 6.5$ can occur along the Morne Piton fault system in the event of a rupture of the full length of the fault (with all segments being considered connected at depth in the present demonstration). Such an event would be tsunamigenic according to numerical simulation results. The multisegment tsunami modeling illustrates how submarine morphological and structural features influence the propagation pattern of the tsunami, leading to interference and resonance and an increase in the tsunami threat on nearby islands. It also highlights a resonance effect within the Les Saintes islands which has not been discussed and may be a potential explanation for the so-far unreproduced run-up values of the 2004 tsunami. At a regional scale we evidenced that several other regional faults, such as the Montserrat–Havers–Bouillante fault, the Gosier fault and the Karukera spur border fault, may also be tsunamigenic. Indeed, although they have the potential to produce relatively low magnitude (< 7) earthquakes, their rupture could occur at shallow depth and close to a highly populated coast. Therefore, scenarios with arc and forearc crustal fault ruptures must be integrated within their tsunami hazard assessment plan. For that, it is necessary to have a better understanding of onshore–offshore structural and seismogenic patterns of each individual major faults system as the regional low strain rate leads to a large recurrence time of tsunamigenic earthquakes (> 1000 years), i.e., much greater than the historical record. In addition, these earthquakes could also have the capacity to destabilize the sedimentary layers at the edge of plateaus and canyons, triggering submarine mass failures, and are also capable of triggering large but more localized tsunamis.

Code and data availability. Litto3D data can be found at https://services.data.shom.fr/geonetwork/srv/fre/catalog.search#/metadata/BATHYMETRIE_LITTO3D_GUAD_2016.xml (Shom-IGN, 2019).

French oceanographic fleet data can be obtained on demand via the Sismer online interface following the cruise DOI for Aguadomar, https://doi.org/10.17600/98010120 (Deplus, 1998); Sismantilles, https://doi.org/10.17600/1080060 (Hirn, 2001) and https://doi.org/10.17600/7010020 (Laigle et al., 2007); and KaShallow, https://doi.org/10.17600/9020010 (Lebrun, 2009).

Requests for the GEOBERYX03 data must be addressed to the BRGM.

Some figures were prepared using the Generic Mapping Tools version 6 software (https://www.generic-mapping-tools.org, Wessel et al., 2019).

Supplement. The supplement related to this article is available online at: https://doi.org/10.5194/nhess-24-3129-2024-supplement.

Author contributions. MP: conceptualization; investigation; visualization; data curation; formal analysis; methodology; writing (original draft); writing (review and editing). JR: conceptualization; investigation; data curation; formal analysis; methodology; writing (original draft); writing (review and editing). JFL: formal analysis; investigation; resources; writing (review and editing). IT: formal analysis; investigation; resources; writing (original draft); writing (review and editing). OF: validation; writing (review and editing). SM: validation; writing (review and editing). MAG: investigation; validation; writing (review and editing). LM: resources; writing (review and editing). JJC: conceptualization; investigation; writing (original draft); writing (review and editing).

Competing interests. The contact author has declared that none of the authors has any competing interests.

Disclaimer. Publisher's note: Copernicus Publications remains neutral with regard to jurisdictional claims made in the text, published maps, institutional affiliations, or any other geographical representation in this paper. While Copernicus Publications makes every effort to include appropriate place names, the final responsibility lies with the authors.

Acknowledgements. We are grateful to Cecile Deplus (IPGP), Alfred Hirn (IPGP) and Mireille Laigle (GeoAzur) for providing Aguadomar and Sismantilles seismic and bathymetry data and to Isabelle Thinon and Pol Gennoc (BRGM) for providing the GEOBERYX03 seismic data. We warmly thank José A. Álvarez-Gómez and the anonymous reviewer for their constructive comments and the editor Rachid Omira for handling our paper.

Financial support. The KaShallow project was supported by the French national program DyETI from INSU-CNRS and by the European Interreg IIIB "Caribbean Space" fund engaged in Guadeloupe with the European Regional Development Fund (ERDF) projects (op. 30-700) and the region of Guadeloupe. Jean Roger has received financial support from the New Zealand's Strategic Science Investment Fund (SSIF). Melody Philippon has received financial support from the ANR SUBUTTEC, ANR-23-CE01-0028.

Review statement. This paper was edited by Rachid Omira and reviewed by José A. Alvarez-Gómez and one anonymous referee.

References

Accary, F. and Roger, J.: Tsunami catalog and vulnerability of Martinique (Lesser Antilles, France), Science of Tsunami Hazards, 29, 3, ISSN 8755-6839 (Print), 2168-6009 (Online), 2010.

Ajvazi, B. and Czimber, K.: A comparative analysis of different DEM interpolation methods in GIS: case study of Rahovec, Kosovo, Geodesy and Cartography, 45, 43–48, https://doi.org/10.3846/gac.2019.7921, 2019.

Álvarez-Gómez, J. A., Gutiérrez, O. Q. G., Aniel-Quiroga, Í., and González, M.: Tsunamigenic potential of outer-rise normal faults at the Middle America trench in Central America, Tectonophysics, 574, 133–143, https://doi.org/10.1016/j.tecto.2012.08.014, 2012.

Arun, P. V.: A comparative analysis of different DEM interpolation methods, The Egyptian Journal of Remote Sensing and Space Science, 16, 133–139, https://doi.org/10.1016/j.ejrs.2013.09.001, 2013.

Barkan, R. and ten Brink, U.: Tsunami simulations of the 1867 virgin island earthquake: Constraints on epicenter location and fault parameterstsunami simulations of the 1867 virgin island earthquake: Constraints on epicenter location, B. Seismol. Soc. Am., 100, 995–1009, https://doi.org/10.1785/0120090211, 2010.

Bazin, S., Feuillet, N., Duclos, C., Crawford, W., Nercessian, A., Bengoubou-Valerius, M., Beauducel, F., and Singh, S. C.: The 2004–2005 Les Saintes (French West Indies) seismic aftershock sequence observed with ocean bottom seismometers, Tectonophysics, 489, 91–103, https://doi.org/10.1016/j.tecto.2010.04.005, 2010.

Beck, C., Reyss, J.-L., Leclerc, F., Moreno, E., Feuillet, N., Barrier, L., Beauducel, F., Boudon, G., Clément, V., Deplus, C., Gallou, N., Lebrun, J.-F., Le Friant, A., Nercessian, A., Paterne, M., Pichot, T., and Vidal, C.: Identification of deep subaqueous co-seismic scarps through specific coeval sedimentation in Lesser Antilles: implication for seismic hazard, Nat. Hazards Earth Syst. Sci., 12, 1755–1767, https://doi.org/10.5194/nhess-12-1755-2012, 2012.

Bengoubou-Valerius, M., Bazin, S., Bertil, D., Beauducel, F., and Bosson, A.: CDSA: a new seismological data center for the French Lesser Antilles, Seismol. Res. Lett., 79, 90–102, 2008.

Bernard, P. and Lambert, J.: Subduction and seismic hazard in the northern Lesser Antilles: Revision of the historical seismicity, B. Seismol. Soc. Am., 78, 1965–1983, 1988.

Bernardes, T., Gontijo, I., Andrade, H., Vieira, T. G. C., and Alves, H. M. R.: Digital Terrain Models Derived from SRTM Data and Kriging, in: Innovations in 3D Geo Information Systems, Lec. Not. Geo. Carto., edited by: Abdul-Rahman, A., Zlatanova S., and Coors V., Springer, Berlin, Heidelberg, https://doi.org/10.1007/978-3-540-36998-1_51, 2006.

Bie, L., Rietbrock, A., Hicks, S., Allen, R., Blundy, J., Clouard, V., Collier, J., Davidson, J., Garth, T., Goes, S., Harmon, N., Henstock; T., van Huenen, J., Kendall, M., Krüger, F., Lynch, L., Macpherson, C., Robertson, R., Tait, S., Wilknison, J., and Wilson, M.: Along-arc heterogeneity in local seismicity across the Lesser Antilles subduction zone from a dense ocean-bottom seismometer network, Seismol. Res. Lett., 91, 237–247, https://doi.org/10.1785/0220190147, 2020.

Biggs, J. and Wright, T. J.: How satellite InSAR has grown from opportunistic science to routine monitoring over the last decade, Nat. Commun., 11, 1–4, https://doi.org/10.1038/s41467-020-17587-6, 2020.

Bilek, S. L.: Invited review paper: Seismicity along the South American subduction zone: Review of large earthquakes, tsunamis, and subduction zone complexity, Tectonophysics, 495, 2–14, https://doi.org/10.1016/j.tecto.2009.02.037, 2010.

Boucard, M., Marcaillou, B., Lebrun, J. F., Laurencin, M., Klingelhoefer, F., Laigle, M., Lallemand, S., Schenini, L., Graindorge, D., Cornee, J. J., Münch, P., and Philippon, M.: Paleogene V-shaped basins and Neogene subsidence of the Northern Lesser Antilles Forearc, Tectonics, 40, e2020TC006524, https://doi.org/10.1029/2020TC006524, 2021.

Bouysse, P. and Mascle, A.: Sedimentary Basins and Petroleum Plays Around the French Antilles, in: Hydrocarbon and Petroleum Geology of France, edited by: Mascle, A., Spe. Pub. EAPG, vol. 4, Springer, Berlin, Heidelberg, https://doi.org/10.1007/978-3-642-78849-9_32, 1994.

Bouysse, P., Garrabé, F., Mauboussin, T., Andreieff, P., Battistini, R., Carlier, P., Hinschberger, F., and Rodet, J.: Carte géologique du département de la Guadeloupe, Notice explicative: Marie-Galante et îlets de la Petite-Terre, scale 1:50,000. – BRGM, Orléans, France, 1993.

Chadha, R. K., Latha, G., Yeh, H., Peterson, C., and Katada, T.: The tsunami of the great Sumatra earthquake of $M_{9.0}$ on 26 December 2004 – Impact on the east coast of India, Curr. Sci.-India, 88, 1297–1301, 2005.

Chen, J. M., Liang, D., and Tang, H.: Interaction between tsunami waves and isolated conical islands, J. Coastal Res., 28, 1270–1278, 2012.

Colon Useche, S., Clouard, V., Ioualalen, M., Audemard, F., and Monfret, T.: Simulation of tsunami inundation for the island of Martinique to nearby large earthquakes, B. Seismol. Soc. Am., 113, 252–267, https://doi.org/10.1785/0120220093, 2023.

Cordrie, L., Gailler, A., Escartín, J., Feuillet, N., and Heinrich, P.: Simulation of the 2004 tsunami of Les Saintes in Guadeloupe (Lesser Antilles) using new source constraints, Nat. Hazards, 103, 2103–2129, https://doi.org/10.1007/s11069-020-04073-x, 2020.

Cornée, J. J., Leticée, J. L., Münch, P., Quillevere, F., Lebrun, J. F., Moissette, P., Braga, C., Melinte-Dobrinescu, M., De Min, L., Oudet, J., and Randrianasolo, A.: Sedimentology, palaeoenvironments and biostratigraphy of the Pliocene–Pleistocene carbonate platform of Grande-Terre (Guadeloupe, Lesser Antilles forearc), Sedimentology, 59, 1426–1451, https://doi.org/10.1111/j.1365-3091.2011.01311.x, 2012.

Cornée, J. J., Münch, P., Philippon, M., Boudagher-Fadel, M., Quillévéré, F., Melinte-Dobrinescu, M., Lebrun, J. F., Meyer, S., Montheil, L., Lallemand, S., Marcailou, B., Laurencin, M., Legndre, L., Garrocq, C., Boucard, M., Beslier, M. O., Laigle, M., Schenini, L., Fabre, P. H., and Marivaux, L.: Lost islands in the northern Lesser Antilles: possible milestones in the Cenozoic dispersal of terrestrial organisms between South-America and the Greater Antilles, Earth-Sci. Rev., 217, 103617, https://doi.org/10.1016/j.earscirev.2021.103617, 2021.

Cornée, J. J., De Min, L., Lebrun, J. F., Quillévéré, F., Melinte-Dobrinescu, M., BouDagher-Fadel, M., Montheil, L., Marcaillou, B., Thinon, I., and Philippon M.: Paleogeographic evolution and vertical motion of the central Lesser Antilles forearc since the Early Miocene: A potential driver for land fauna dis-

persals between the Americas, Mar. Petrol. Geol., 152, 106264, https://doi.org/10.1016/j.marpetgeo.2023.106264, 2023.

Dao, M. H. and Tkalich, P.: Tsunami propagation modelling – a sensitivity study, Nat. Hazards Earth Syst. Sci., 7, 741–754, https://doi.org/10.5194/nhess-7-741-2007, 2007.

Delpey, M., Lastiri, X., Abadie, S., Roeber, V., Maron, P., Liria, P., and Mader, J.: Characterization of the wave resource variability in the French Basque coastal area based on a high-resolution hindcast, Renew. Energ., 178, 79–95, https://doi.org/10.1016/j.renene.2021.05.167, 2021.

DeMets, C., Jansma, P. E., Mattioli, G. S., Dixon, T. H., Farina, F., Bilham, R., Calais., E., and Mann, P.: GPS geodetic constraints on Caribbean-North America plate motion, Geophys. Res. Lett., 27, 437–440, https://doi.org/10.1029/1999GL005436, 2000.

De Min, L., Lebrun, J. F., Cornée, J. J., Münch, P., Léticée, J. L., Quillévéré, F., Melinte-Dobrinescu, M., Randrianasolo, A., Marcaillou, B., and Zami, F.: Tectonic and sedimentary architecture of the Karukéra spur: A record of the Lesser Antilles fore-arc deformations since the Neogene, Mar. Geol., 363, 15–37, https://doi.org/10.1016/j.margeo.2015.02.007, 2015.

Deplus, C.: AGUADOMAR cruise, RV *L'Atalante* , French Oceanographic Cruises [data set], https://doi.org/10.17600/98010120, 1998.

Deplus, C., Le Friant, A., Boudon, G., Komorowski, J. C., Villemant, B., Harford, C., Ségoufin, J., and Cheminée, J. L.: Submarine evidence for large-scale debris avalanches in the Lesser Antilles Arc, Earth Planet. Sc. Lett., 192, 145–157, 2001.

Dix, C. H.: Seismic Velocities from Surface Measurements, Geophysics, 20, 68–86, https://doi.org/10.1190/1.1438126, 1955.

do Carmo, J. S. A.: Dominant processes that amplify the swell towards the coast: the Nazaré Canyon and the giant waves, Research, Society and Development, 11, e578111133804, https://doi.org/10.33448/rsd-v11i11.33804, 2022.

Escartín, J., Leclerc, F., Olive, J. A., Mevel, C., Cannat, M., Petersen, S., Augustin, N., Feuillet, N., Deplus, C., Bezos, A., Bonnemains, D., Chavagnac, V., Choi, Y., Godard, M., Haaga, K., Hamelin, C., Ildefonse, B., Jamieson, J. W., John, B. E., Leleu, T., MacLead, C. J., Massot-Campos, M., Nomikou, P., Paquet, M., Tominaga, M., Triebe, L., Campos, R., Gracias, N., Garcia, R., Andreani, M., and Vilaseca, G.: First direct observation of coseismic slip and seafloor rupture along a submarine normal fault and implications for fault slip history, Earth Planet. Sc. Lett., 450, 96–107, https://doi.org/10.1016/j.epsl.2016.06.024, 2016.

Escartín, J., Leclerc, F., Nathalie, F., Le Friant, A., Billant, J., Olive, J. A. L., Henri, M., Andreani, M., Arnaubec, A., Dano, A., Delorme, A., Deplus, C., Fournasson, M. L., Gini, C., Gracias, N., Hamelin, C., Istenic, K., Komorowski, J. C., Marchand C., Mevel, C., Onstad, S., Quidelleur, X., and Garcia, R.: Mapping the Mw6.3 2004 Les Saintes earthquake seafloor rupture with deep-sea vehicles: Length, displacement, nature, and links between coseismic deformation and erosion/sedimentation, in: AGU Fall Meeting Abstracts, Vol. 2018, EP51D-1851, https://ui.adsabs.harvard.edu/abs/2018AGUFMEP51D1851E/abstract (last access: September 2024), 2018.

Feuillet, N.: Sismotectonique des Petites Antilles: Liaison entre activité sismique et volcanique, Doctoral dissertation, Paris 7, https://theses.fr/2000PA077079 (last access: September 2024), 2000.

Feuillet, N., Manighetti, I., and Tapponnier, P.: Extension active perpendiculaire à la subduction dans l'arc des Petites Antilles (Guadeloupe, Antilles françaises), CR Acad. Sci. II A, 333, 583–590, 2001.

Feuillet, N., Manighetti, I., Tapponnier, P., and Jacques, E.: Arc parallel extension and localization of volcanic complexes in Guadeloupe, Lesser Antilles, J. Geophys. Res.-Sol. Ea., 107, 2331, https://doi.org/10.1029/2001JB000308, 2002.

Feuillet, N., Tapponnier, P., Manighetti, I., Villemant, B., and King, G. C. P.: Differential uplift and tilt of Pleistocene reef platforms and Quaternary slip rate on the Morne-Piton normal fault (Guadeloupe, French West Indies), J. Geophys. Res.-Sol. Ea, 109, B02404, https://doi.org/10.1029/2003JB002496, 2004.

Feuillet, N., Leclerc, F., Tapponnier, P., Beauducel, F., Boudon, G., Le Friant, A., Deplus, C., Lebrun, J. F., Nercessian, A., Saurel, J. M., and Clément, V.: Active faulting induced by slip partitioning in Montserrat and link with volcanic activity: New insights from the 2009 GWADASEIS marine cruise data, Geophys. Res. Lett., 37, L00E15, https://doi.org/10.1029/2010GL042556, 2010.

Feuillet, N., Beauducel, F., and Tapponnier, P.: Tectonic context of moderate to large historical earthquakes in the Lesser Antilles and mechanical coupling with volcanoes, J. Geophys. Res.-Sol. Ea, 116, B10308, https://doi.org/10.1029/2011JB008443, 2011.

Fujita, M., Ishikawa, T., Mochizuki, M., Sato, M., Toyama, S. I., Katayama, M., Kawai, K., Mastumoto, Y., Yabuki, T., Asada, A., and Colombo, O. L.: GPS/Acoustic seafloor geodetic observation: method of data analysis and its application, Earth Planets Space, 58, 265–275, https://doi.org/10.1186/BF03351923, 2006.

Garrabe, F. and Andreieff P.: Notice explicative de la feuille de la Grande-Terre- Carte géologique au 1/50 000, Département de la Guadeloupe, BRGM, 1988.

GEBCO Compilation Group: GEBCO 2021 Grid, NERC EDS British Oceanographic Data Centre NOC [data set], https://doi.org/10.5285/c6612cbe-50b3-0cff-e053-6c86abc09f8f, 2021.

Geli, L., Çağatay, N., Gasperini, L., Favali, P., Henry, P., and Çifçi, G.: ESONET WP4-Demonstration Missions. MARMARA-DM final report, https://archimer.ifremer.fr/doc/00032/14324/ (last access: October 2022), 2011.

Goldfinger, C., Nelson, C. H., Morey, A. E., Johnson, J. E., Patton, J. R., Karabanov, E. B., Gutierrez-Pastor, J., Eriksson, A. T., Gracia, E., Dunhill, G., Enkin, R. J., Dallimore, A., and Vallier, T.: Turbidite event history – Methods and implications for Holocene paleoseismicity of the Cascadia subduction zone, No. 1661-F, US Geological Survey, https://doi.org/10.3133/pp1661F, 2012.

Gonzalez, O. L., Clouard, V., and Zahradnik, J.: Moment tensor solutions along the central Lesser Antilles using regional broadband stations, Tectonophysics, 717, 214–225, https://doi.org/10.1016/j.tecto.2017.06.024, 2017.

Gusman, A. R., Supendi, P., Nugraha, A. D., Power, W., Latief, H., Sunendar, H., Widiyantoro, S., Daryono, Wiyono, S. H., Hakim, A., Muhari, A., Wang, X., Burbidge, D., Palgunadi, K., Hamling, I., and Daryono, M. R.: Source model for the tsunami inside Palu Bay following the 2018 Palu earthquake, Indonesia, Geophys. Res. Lett., 46, 8721–8730, https://doi.org/10.1029/2019GL082717, 2019.

Gusman, A. R., Roger, J., Power, W., Fry, B., and Kaneko, Y.: The 2021 Loyalty Islands earthquake (Mw 7.7): Tsunami waveform inversion and implications for tsunami forecasting

for New Zealand. Earth and Space Science, e2022EA002346, https://doi.org/10.1029/2022EA002346, 2022.

Gutscher, M. A., Roger, J., Baptista, M. A., Miranda, J. M., and Tinti, S.: Source of the 1693 Catania earthquake and tsunami (southern Italy): New evidence from tsunami modeling of a locked subduction fault plane, Geophys. Res. Lett., 33, L08309, https://doi.org/10.1029/2005GL025442,, 2006.

Gutscher, M. A., Royer, J. Y., Graindorge, D., Murphy, S., Klingelhoefer, F., Aiken, C., Cattaneo, A., Barreca, G., Quetel, L., Riccobene, G., Petersen, F., Urlaub, M., Krastel, S., Gross, F., Kopp, H., Margheriti, L., and Beranzoli, L.: Fiber optic monitoring of active faults at the seafloor: I the FOCUS project, Photoniques Special EOS Issue, 32–37, https://doi.org/10.1051/photon/2019S432, 2019.

Gutscher, M.-A., Quetel, L., Cappelli, G., Quillin, J.-G., Nativelle, C., Lebrun, J.-F., and Philippon, M.: Monitoring a commercially operating submarine telecom cable network in the Guadeloupe archipelago (Lesser Antilles) using Brillouin Optical Time Domain Reflectometry (BOTDR), EGU General Assembly 2023, Vienna, Austria, 23–28 Apr 2023, EGU23-8569, https://doi.org/10.5194/egusphere-egu23-8569, 2023.

Hirata, K., Aoyagi, M., Mikada, H., Kawaguchi, K., Kaiho, Y., Iwase, R., Morita, S., Fujisawa, I., Sugioka, H., Mitsuzawa, K., Suyehiro, K., and Fujiwara, N.: Real-time geophysical measurements on the deep seafloor using submarine cable in the southern Kurile subduction zone, IEEE J. Oceanic Eng., 27, 170–181, https://doi.org/10.1109/JOE.2002.1002471, 2002.

Hirn, A.: SISMANTILLES 1 cruise, RV *Nadir*, French Oceanographic Cruises [data set], https://doi.org/10.17600/1080060, 2001.

International Seismological Centre: ISC-GEM Earthquake Catalogue, https://doi.org/10.31905/d808b825, 2023.

IOC-UNESCO: Experts Meeting on Sources of Tsunamis in the Lesser Antilles Fort-de-France, Martinique (France) 18–20 March 2019, Workshop Reports, (291), 55 pp., Open Access version, https://archimer.ifremer.fr/doc/00665/77736/ (last access: October 2022), 2020.

Kido, M., Fujimoto, H., Miura, S., Osada, Y., Tsuka, K., and Tabei, T.: Seafloor displacement at Kumano-nada caused by the 2004 off Kii Peninsula earthquakes, detected through repeated GPS/Acoustic surveys, Earth Planets Space, 58, 911–915, https://doi.org/10.1186/BF03351996, 2006.

Kopp, H., Weinzierl, W., Becel, A., Charvis, P., Evain, M., Flueh, E. R., Gailler, A., Galve, A., Hirn, A., Kandilarov, D., Klaeschen, D., Laigle, M., Papenberg, C., Planert, L., and Roux, E.: Deep structure of the central Lesser Antilles Island Arc: relevance for the formation of continental crust, Earth Planet. Sc. Lett., 304, 121–134, https://doi.org/10.1016/j.epsl.2011.01.024, 2011.

Laigle, M., Lebrun, J.-F., and Hirn, A.: SISMANTILLES 2 cruise, RV *L'Atalante*, French Oceanographic Cruises [data set], https://doi.org/10.17600/7010020, 2007.

Lander, J. F. and Whiteside, L. S.: Caribbean tsunamis: an initial history, In Caribbean Tsunami Workshop, Kingstone, Jamaïca, June, 11–13, https://www.proyecto1867.com/uploads/8/6/3/9/86396506/lander__1997_.pdf (last access: August 2024), 1997.

Lander, J. F., Whiteside, L. S., and Lockridge, P. A.: Two decades of global tsunamis, Science of Tsunami Hazards, 21, 1, https://www.ngdc.noaa.gov/hazard/data/publications/ref1315_lander.pdf (last access: September 2024), 2003.

Lardeaux, J. M., Münch, P., Corsini, M., Cornée, J. J., Verati, C., Lebrun, J. F., Guillevere, F., Melinte-Dobrinescu, M., Leticee, J. L., Fietzke, J., Mazabraud, Y., Cordrey, F., and Randrianasolo, A.: La Désirade island (Guadeloupe, French West Indies): a key target for deciphering the role of reactivated tectonic structures in Lesser Antilles arc building, B. Soc. Géol. Fr., 184, 21–34, https://doi.org/10.2113/gssgfbull.184.1-2.21, 2013.

Lebrun, J.-F.: KASHALLOW 2 cruise, RV *Le Suroît*, French Oceanographic Cruises [data set], https://doi.org/10.17600/9020010, 2009.

Lebrun, J.-F., Cornée, J.-J., Münch, P., Guennoc, P., Thinon, I., Begot, J., Mazabraud, Y., Fournier, F., Feuillet, N., and Randrianasolo, A.: La Mission KaShallow 1 – N/O Antéa – 26 avril – 05 Mai – Sismique réflexion haute résolution dans le bassin de Marie-Galante – Avant-arc des Petites Antilles, Rapport de l'Université des Antilles et de la Guyane, 2008.

Leclerc, F., Feuillet, N., and Deplus, C.: Interactions between active faulting, volcanism, and sedimentary processes at an island arc: Insights from Les Saintes channel, Lesser Antilles arc, Geochem. Geophy. Geosy., 17, 2781–2802, https://doi.org/10.1002/2016GC006337, 2016.

Le Friant, A., Heinrich, P., and Boudon, G.: Field survey and numerical simulation of the 21 November 2004 tsunami at Les Saintes (Lesser Antilles), Geophy. Res. Lett., 35, L12308, https://doi.org/10.1029/2008GL034051, 2008.

Le Friant, A., Boudon, G., Arnulf, A., and Robertson, R. E.: Debris avalanche deposits offshore St. Vincent (West Indies): impact of flank-collapse events on the morphological evolution of the island, J. Volcanol. Geoth. Res., 179, 1–10, 2009.

Le Friant, A., Ishizuka, O., Stroncik, N. A., and the Expedition 340 Scientists: Site U1395, Proceedings of the IODP, https://doi.org/10.2204/iodp.proc.340.105.2013, 2013.

Le Friant, A., Lebas, E., Brunet, M., Lafuerza, S., Hornbach, M., Coussens, M., Watt, S., Cassidy, M., Talling, P. J., and IODP 340 Expedition Science Party: Submarine landslides around volcanic islands: A review of what can be learned from the Lesser Antilles Arc, in: Submarine Landslides: Subaqueous Mass Transport Deposits from Outcrops to Seismic Profiles, edited by: Ogata, K., Festa, A., and Pini, G. A., 277–297, https://doi.org/10.1002/9781119500513.ch17, 2019.

Legendre, L., Philippon, M., Münch, P., Leticee, J. L., Noury, M., Maincent, G., Cornee, J. J., Caravati, A., Lebrun, J. F., and Mazabraud, Y.: Trench bending initiation: Upper plate strain pattern and volcanism. insights from the Lesser Antilles arc, St. Barthelemy island, French West Indies, Tectonics, 37, 2777–2797, 2018.

Lehu, R., Lallemand, S., Ratzov, G., Babonneau, N., Hsu, S. K., Lin, A. T., and Dezileau, L.: An attempt to reconstruct 2700 years of seismicity using deep-sea turbidites offshore eastern Taiwan, Tectonophysics, 692, 309–324, https://doi.org/10.1016/j.tecto.2016.04.030, 2016.

Leonard, M.: Earthquake fault scaling: Self-consistent relating of rupture length, width, average displacement, and moment release, B. Seismol. Soc. Am., 100, 1971–1988, 2010.

Leticée, J. L., Cornee, J. J., Münch, P., Fietzke, J., Philippon, M., Lebrun, J. F., De Min, L., and Randrianasolo, A.: Decreasing uplift rates and Pleistocene marine terraces settlement in the central

lesser Antilles fore-arc (La Désirade Island, 16° N), Quatern. Int., 508, 43–59, https://doi.org/10.1016/j.quaint.2018.10.030, 2019.

Leslie, S. C. and Mann, P.: Giant submarine landslides on the Colombian margin and tsunami risk in the Caribbean Sea, Earth Planet. Sci. Lett., 449, 382–394, 2016.

Lewis, K. B.: Quaternary sedimentation on the Hikurangi oblique-subduction and transform margin, New Zealand, Sedimentation in oblique-slip mobile zones, Wiley, 171–189, https://doi.org/10.1002/9781444303735.ch10, 1980.

Liu, P. L. F., Woo, S. B., and Cho, Y. S.: Computer programs for tsunami propagation and inundation, Ithaca (NY), Cornell University, Technical Report, https://tsunamiportal.nacse.org/documentation/COMCOT_tech.pdf (last access: August 2024), 1998.

Mallet, R.: Catalogue of Recorded Earthquakes from 1606 B.C. to A.D. 1850, Part I,1606 B.C. to 1755 A.D., Report of the 22nd Meeting of the British Association for the Advancement of Science, held in Belfast, Sept. 1852, John Murray, London, 177 pp., 1853.

Mallet R.: Catalogue of Recorded Earthquakes from 1606 B.C. to A.D. 1850, Part II, 1755 A.D. to 1784 A.D., Report of the 23Td meeting of the British Association for the Advancement of Science, held in Hull, September 1853, John Murray, London, 118–212, 1854.

Mallet R.: Catalogue of Recorded Earthquakes from 1606 B.C. to A.D. 1850, Part III, 1784 A.D. to 1842 A.D., Report of the 24th Meeting of the British Association for the Advancement of Science, John Murray, London, 326 pp., http://storing.ingv.it/cfti/cfti5/pdf_T/000090-060028_T.pdf (last access: September 2024), 1855.

Martins, I., Vitorino, J., and Almeida, S.: The Nazare Canyon observatory (W Portugal) real-time monitoring of a large submarine canyon, in: OCEANS'10 IEEE SYDNEY, Sydney, NSW, Australia, 2010, https://doi.org/10.1109/OCEANSSYD.2010.5603854, 2010.

Martínez-Loriente, S., Sallarès, V., and Gràcia, E.: The Horseshoe Abyssal plain Thrust could be the source of the 1755 Lisbon earthquake and tsunami, Commun. Earth Environ., 2, 145, https://doi.org/10.1038/s43247-021-00216-5, 2021.

Massin, F., Clouard, V., Vorobieva, I., Beauducel, F., Saurel, J. M., Satriano, C., Bouin, M. P., and Bertil, D.: Automatic picking and probabilistic location for earthquake assessment in the lesser antilles subduction zone (1972–2012), C. R. Geosci., 353, 187–209, https://doi.org/10.5802/crgeos.81, 2021.

McCalpin, J. P.: Paleoseismology, Academic Press, London, p. 583, ISBN-10: 0123735769, 1996.

Münch, P., Lebrun, J. F., Cornée, J. J., Thinon, I., Guennoc, P., Marcaillou, B. J., Begot, J., Bertrand, G., Bes De Berc, S., Biscarrat, K., Claud, C., De Min, L., Fournier, F., Gailler, L., Grandorge, D., Leticee, J. L., Marie, L., Mazabraud, Y., Melinte-Dobrinescu, M., Moisette, P., Quilevere, F., Verati, C., and Randrianasolo, A.: Pliocene to Pleistocene carbonate systems of the Guadeloupe archipelago, French Lesser Antilles: a land and sea study (the KaShallow project), B. Soc. Géol. Fr., 184, 99–110, https://doi.org/10.2113/gssgfbull.184.1-2.99, 2013.

Münch, P., Cornee, J. J., Lebrun, J. F., Quillevere, F., Verati, C., Melinte-Dobrinescu, M., Demory, B., Smith, F., Jourdan, J. M., Lardeaux, J. M., De Min, L., Leticee, J. L., and Randrianasolo, A.: Pliocene to Pleistocene vertical movements in the forearc of the Lesser Antilles subduction: insights from chronostratigraphy of shallow-water carbonate platforms (Guadeloupe archipelago), J. Geol. Soc. London, 171, 329–341, https://doi.org/10.1144/jgs2013-005, 2014.

NOAA: National Geophysical Data Center/World Data Service, NOAA [data set], https://doi.org/10.7289/V5PN93H7, 2024.

NASA Shuttle Radar Topography Mission (SRTM): Shuttle Radar Topography Mission (SRTM) Global, OpenTopography [data set], https://doi.org/10.5069/G9445JDF, 2013.

Nikolkina, I., Zahibo, N., and Pelinovsky, E.: Tsunami in Guadeloupe (Caribbean Sea), The Open Oceanography Journal, 4, 44–49, https://doi.org/10.2174/1874252101004010044, 2010.

Okada, Y.: Surface deformation due to shear and tensile faults in a half-space, B. Seismol. Soc. Am., 75, 1135–1154, https://doi.org/10.1785/BSSA0750041135, 1985.

O'loughlin, K. F. and Lander, J. F.: Caribbean tsunamis: a 500-year history from 1498–1998, 20, Springer Science & Business Media, ISBN 1-4020-1717-0, 2003.

Padron, C., Klingelhoefer, F., Marcaillou, B., Lebrun, J. F., Lallemand, S., Garrocq, C., Laigle, M., Roest, W. R., Beslier, M. O., Schenini, L., Graindorge, D., Gay, A., Audemard, F., Munch., P., and GARANTI Cruise Team.: Deep structure of the Grenada Basin from wide-angle seismic, bathymetric and gravity data, J. Geophys. Res.-Sol. Ea., 126, e2020JB020472. https://doi.org/10.1029/2020JB020472, 2021.

Paris, R., Sabatier, P., Biguenet, M., Bougouin, A., André, G., and Roger, J.: A tsunami deposit at Anse Meunier, Martinique Island: evidence of the 1755 CE Lisbon tsunami and implication for hazard assessment, Mar. Geol., 439, 106561, https://doi.org/10.1016/j.margeo.2021.106561, 2021.

Petersen, F., Kopp, H., Lange, D., Hannemann, K., and Urlaub, M.: Measuring tectonic seafloor deformation and strain-build up with acoustic direct-path ranging, J. Geodyn., 124, 14–24, https://doi.org/10.1016/j.jog.2019.01.002, 2019.

Philippon, M. and Corti, G.: Obliquity along plate boundaries, Tectonophysics, 693, 171–182, https://doi.org/10.1016/j.tecto.2016.05.033, 2016.

Prasetya, G., Beavan, J., Wang, X., Reyners, M., Power, W., Wilson, K., and Lukovic, B.: Evaluation of the 15 July 2009 Fjorland, New Zealand tsunami in the source region, Pure Appl. Geophys., 168, 1973–1987, https://doi.org/10.1007/s00024-011-0282-6, 2011.

Roger, J., Allgeyer, S., Hébert, H., Baptista, M. A., Loevenbruck, A., and Schindelé, F.: The 1755 Lisbon tsunami in Guadeloupe Archipelago: source sensitivity and investigation of resonance effects, The Open Oceanography Journal, 4, 58–70, https://doi.org/10.2174/1874252101004010058, 2010.

Roger, J., Baptista, M. A., Sahal, A., Accary, F., Allgeyer, S., and Hébert, H.: The transoceanic 1755 Lisbon tsunami in Martinique, Pure Appl. Geophys., 168, 1015–1031, https://doi.org/10.1007/s00024-010-0216-8, 2011.

Roger, J., Dudon, B., and Zahibo, N.: Tsunami hazard assessment of Guadeloupe Island (F.W.I.) related to a megathrust rupture on the Lesser Antilles subduction interface, Nat. Hazards Earth Syst. Sci., 13, 1169–1183, https://doi.org/10.5194/nhess-13-1169-2013, 2013.

Roger, J., Pelletier, B., and Aucan, J.: Update of the tsunami catalogue of New Caledonia using a decision table based on seismic

data and marigraphic records, Nat. Hazards Earth Syst. Sci., 19, 1471–1483, https://doi.org/10.5194/nhess-19-1471-2019, 2019.

Roger, J., Pelletier, B., Gusman, A., Power, W., Wang, X., Burbidge, D., and Duphil, M.: Potential tsunami hazard of the southern Vanuatu subduction zone: tectonics, case study of the Matthew Island tsunami of 10 February 2021 and implication in regional hazard assessment, Nat. Hazards Earth Syst. Sci., 23, 393–414, https://doi.org/10.5194/nhess-23-393-2023, 2023.

Roger, J. H., Bull, S., Watson, S. J., Mueller, C., Hillman, J. I., Wolter, A., Lamarche, G., Power, W., Lane, E., Woelz, S., and Davidson, S.: A review of approaches for submarine landslide-tsunami hazard identification and assessment, Mar. Petrol. Geol., 162, 106729, https://doi.org/10.1016/j.marpetgeo.2024.106729, 2024.

Ruiz, M., Galve, A., Monfret, T., Sapin, M., Charvis, P., Laigle, M., Evain, M., Hirn, A., Flueh, E., Gallart, K., Diaz, J., Lebrun, J. F., and Lebrun, J. F.: Seismic activity offshore Martinique and Dominica islands (Central Lesser Antilles subduction zone) from temporary onshore and offshore seismic networks, Tectonophysics, 603, 68–78, https://doi.org/10.1016/j.tecto.2011.08.006, 2013.

Salichon, J., Lemoine, A., and Aochi, H.: Validation of teleseismic inversion of the 2004 Mw6.3 Les Saintes, Lesser Antilles, earthquake by 3D finite-difference forward modelling, B. Seismol. Soc. Am. 99, 3390–3401, https://doi.org/10.1785/0120080315, 2009.

Satake, K. and Tanioka, Y.: Sources of tsunami and tsunamigenic earthquakes in subduction zones, Pure Appl. Geophys., 154, 467–483, https://doi.org/10.1785/0120120306, 1999.

Seibert, C., Feuillet, N., Ratzov, G., Beck, C., and Cattaneo, A.: Seafloor morphology and sediment transfer in the mixed carbonate-siliciclastic environment of the Lesser Antilles forearc along Barbuda to St. Lucia, Mar. Geol., 428, 106242, https://doi.org/10.1016/j.margeo.2020.106242, 2020.

Shom-IGN: Litto3D® – Saint-Barthélemy 2019, Shom-IGN [data set], https://services.data.shom.fr/geonetwork/srv/fre/catalog.search#/metadata/BATHYMETRIE_LITTO3D_GUAD_2016.xml (last access: September 2024), 2019.

Smith, M. S. and Shepherd, J. B.: Tsunami waves generated by volcanic landslides: an assessment of the hazard associated with Kick'em Jenny, Geol. Soc. London, Spe. Pub., 110, 115–123, 1996.

Symithe, S. J., Calais, E., Haase, J. S., Freed, A. M., and Douilly, R.: Coseismic slip distribution of the 2010 M 7.0 Haiti earthquake and resulting stress changes on regional faults, B. Seismol. Soc. Am., 103, 2326–2343, https://doi.org/10.1785/0120120306, 2013.

ten Brink, U., Danforth, W., Polloni, C., Andrews, B., Llanes, P., Smith, S., Parker, E., and Uozumi, T.: New seafloor map of the Puerto Rico trench helps assess earthquake and tsunami hazards, Eos T. Am. Geophys. Un., 85, 349–360, https://doi.org/10.1029/2004EO370001, 2004.

Terrier, M., Combes, P., de Carbon, D., Grellet, B., and Sedan, O.: Failles Actives et Evaluation de L'Alea Sismique: Prise en compte des failles actives dans l'aménagement du territoire aux Antilles (Martinique et Guadeloupe), Partie 1: Identification des systèmes de failles actives dans l'archipel de la Guadeloupe et l'île de la Martinique, Rapport BRGM/RP-51258-FR, 118 pp., 30 figures, 8 tableaux, 4 annexes, http://infoterre.brgm.fr/rapports/RP-51564-FR.pdf (last access: August 2024), 2002.

Teeuw, R., Rust, D., Solana, C., Dewdney, C., and Robertson, R.: Large coastal landslides and tsunami hazard in the Caribbean. Eos T. Am. Geophys. Un., 90, 81–82, 2009.

Thingbaijam, K. K. S., Mai, P. M., and Goda, K.: New Empirical Earthquake Source-Scaling Laws, B. Seismol. Soc. Am., 107, 2225–2246, https://doi.org/10.1785/0120170017, 2017.

Thinon, I. and Bitri, A.: GEOBERYX03 cruise, RV Beryx, Catalogue des campagnes à la mer, Seadatanet webportal (SISM_BGM_FI352003000010) [data set], https://cdi.seadatanet.org/ (last access: September 2024), 2003.

Thinon, I., Bitri, A., Guennoc, P., and Truffert, C.: Levés sismique et magnétique du plateau occidental de l'île de Basse-Terre, Guadeloupe (Campagne Geoberyx03), Apports aỉ la compreìhension du contexte structural du champ geìothermique de Bouillante, BRGM/RP-53152-FR, 77, http://infoterre.brgm.fr/rechercher/search.htm (last access: October 2022), 2004.

Thinon, I., Guennoc, P., Bitri, A., and Truffert C.: Study of the Bouillante Bay (West Basse-Terre Island shelf): contribution of geophysical surveys to the understanding of the structural context of Guadeloupe (French West Indies – Lesser Antilles), B. Soc. Geol. Fr., 181, 51–65, https://doi.org/10.2113/gssgfbull.181.1.51, 2010.

TL/ICMMG: Global Historical Tsunami Database. Institute of Computational Mathematics and Mathematical Geophysics SB RAS Tsunami Laboratory, Novosibirsk, Russia, http://tsun.sscc.ru/gtdb/default.aspx (last access: 1 February 2023), 2023.

Tronin, A. A.: Satellite remote sensing in seismology. A review, Remote Sensing, 2, 124–150, https://doi.org/10.3390/rs2010124, 2009.

USGS: Advanced National Seismic System (ANSS) Comprehensive Catalog, U.S. Geological Survey, USGS [data set], https://doi.org/10.5066/F7MS3QZH, 2017.

van Rijsingen, E. M., Calais, E., Jolivet, R., de Chabalier, J. B., Jara, J., Symithe, S., Robertson, R., and Ryan, G. A.: Inferring interseismic coupling along the lesser antilles arc: A Bayesian approach, J. Geophys. Res.-Sol. Ea., 126, e2020JB020677, https://doi.org/10.1029/2020JB020677, 2021.

Wallace, T. C., Helmberger, D. V., and Ebel, J. E.: A broadband study of the 13 August 1978 Santa Barbara earthquake, B. Seismol. Soc. Am., 71, 1701–1718, https://pubs.geoscienceworld.org/ssa/bssa/article-abstract/71/6/1701/102037/A-broadband-study-of-the-13-August-1978-Santa (last access: September 2024), 1981.

Wang, X.: Numerical modelling of surface and internal waves over shallow and intermediate water, PhD thesis, Cornell University, Ithaca (NY), 245 pp., https://catalog.library.cornell.edu/catalog/6794450 (last access: August 2024), 2008.

Wang, X. and Power, W. L.: COMCOT: a tsunami generation, propagation and run-up model. Lower Hutt (NZ), GNS Science, 121 pp., GNS Science report; 2011/43, https://www.gns.cri.nz/data-and-resources/comcot-a-tsunami-generation-propagation-and-run-up-model/ (last access: August 2024), 2011.

Wang, X., Lukovic, B., Power, W. L., and Mueller, C.: High-resolution inundation modelling with explicit buildings. Lower

Hutt (NZ), GNS Science, 27 pp., GNS Science report 2017/13, https://doi.org/10.21420/G2RW2N, 2017.

Wells, D. L. and Coppersmith, K. J.: New empirical relationships among magnitude, rupture length, rupture width, rupture area, and surface displacement, B. Seismol. Soc. Am., 84, 974–1002, https://doi.org/10.1785/BSSA0840040974, 1994.

Wessel, P., Luis, J. F., Uieda, L., Scharroo, R., Wobbe, F., Smith, W. H. F., and Tian, D.: The Generic Mapping Tools Version 6, Geochem. Geophy. Geosys., 20, 5556–5564, https://doi.org/10.1029/2019GC008515, 2019 (software available at: https://www.generic-mapping-tools.org, last access: September 2024).

Zahibo, N. and Pelinovsky, E. N.: Evaluation of tsunami risk in the Lesser Antilles, Nat. Hazards Earth Syst. Sci., 1, 221–231, https://doi.org/10.5194/nhess-1-221-2001, 2001.

Zahibo, N., Pelinovsky, E., Kurkin, A., and Kozelkov, A.: Estimation of far-field tsunami potential for the Caribbean Coast based on numerical simulation, Science of Tsunami Hazards, 21, 202–222, 2003.

Zahibo, N., Pelinovsky, E., Okal, E., Yalçiner, A., Kharif, C., Talipova, T., and Kozelkov, A.: The earthquake and tsunami of November 21, 2004 at Les Saintes, Guadeloupe, Lesser Antilles, Science of Tsunami Hazards, 23, 25–39, 2005.

Zhang, L., Baba, K., Liang, P., Shimizu, H., and Utada, H.: The 2011 Tohoku Tsunami observed by an array of ocean bottom electromagnetometers, Geophys. Res. Lett., 41, 4937–4944, https://doi.org/10.1002/2014GL060850, 2014.